HHS Public Access

Author manuscript

Nat Immunol. Author manuscript; available in PMC 2022 December 01.

Published in final edited form as:

Nat Immunol. 2021 December ; 22(12): 1563–1576. doi:10.1038/s41590-021-01064-3.

Disrupting Roquin-1 interaction with Regnase-1 induces autoimmunity and enhances antitumor responses

Gesine Behrens[1,14], **Stephanie L. Edelmann**[2,14], **Timsse Raj**[1,14], **Nina Kronbeck**[1], **Thomas Monecke**[3], **Elena Davydova**[4], **Elaine H. Wong**[1], **Lisa Kifinger**[2], **Florian Giesert**[5], **Martin E. Kirmaier**[6,7], **Christine Hohn**[1], **Laura S. de Jonge**[2], **Mariano Gonzalez Pisfil**[8], **Mingui Fu**[9], **Sebastian Theurich**[6,7], **Stefan Feske**[10], **Naoto Kawakami**[11], **Wolfgang Wurst**[5,12,13], **Dierk Niessing**[3,4], **Vigo Heissmeyer**[1,2]

[1]Institute for Immunology, Biomedical Center (BMC), Faculty of Medicine, Ludwig-Maximilians-Universität in Munich, Planegg-Martinsried, Germany.

[2]Research Unit Molecular Immune Regulation, Helmholtz Zentrum München, Munich, Germany.

[3]Institute of Pharmaceutical Biotechnology, Ulm University, Ulm, Germany.

[4]Institute of Structural Biology, Helmholtz Zentrum München, Neuherberg, Germany.

[5]Institute of Developmental Genetics, Helmholtz Zentrum München, Neuherberg, Germany.

[6]Cancer and Immunometabolism Research Group at the Gene Center, Ludwig-Maximilians-Universität in Munich, Munich, Germany.

[7]Department of Medicine III, LMU University Hospital, Ludwig-Maximilians-Universität in Munich, Munich, Germany.

[8]Core Facility Bioimaging and Walter-Brendel-Centre of Experimental Medicine at the Biomedical Center, Ludwig-Maximilians-Universität in Munich, Planegg-Martinsried, Germany.

Correspondence and requests for materials should be addressed to Vigo Heissmeyer. vigo.heissmeyer@med.uni-muenchen.de.

Author contributions

G.B., S.L.E, T.R., N. Kronbeck and V.H. conceived the project and designed experiments with input from S.F., D.N. and N. Kawakami. G.B., S.L.E., T.R. and N. Kronbeck performed and analyzed most of the experiments. T.M. performed in vitro pulldown experiments, E.D. performed EMSA experiments and SPR assays and E.W. performed ELISA measurements. L.K. performed NanoBret assays and, together with M.G.P., FLIM/FRET experiments and C.H. contributed to kinetic expression analyses. M.K. and L.D.J. performed seahorse measurements with supervision from S.T. F.G. and W.W. generated mice expressing Roquin-1^{L209Y} and M.F. provided the *Zc3h12a*^{fl} mouse line. The manuscript was written by G.B. and V.H. with critical input from S.F.

Reporting Summary. Further information on research design is available in the Nature Research Reporting Summary linked to this article.

Online content

Any methods, additional references, Nature Research reporting summaries, source data, extended data, supplementary information, acknowledgements, peer review information; details of author contributions and competing interests; and statements of data and code availability are available at https://doi.org/10.1038/s41590-021-01064-3.

Extended data is available for this paper at https://doi.org/10.1038/s41590-021-01064-3.

Supplementary information The online version contains supplementary material available at https://doi.org/10.1038/s41590-021-01064-3.

Competing interests

The authors declare no competing interests.

[9]Department of Basic Medical Science, School of Medicine, University of Missouri-Kansas City, Kansas City, MO, USA.

[10]Department of Pathology, New York University School of Medicine, New York, NY, USA.

[11]Institute of Clinical Neuroimmunology, University Hospital and Biomedical Center, Ludwig-Maximilians-Universität in Munich, Planegg-Martinsried, Germany.

[12]German Center for Neurodegenerative Diseases (DZNE) Site Munich, Munich, Germany.

[13]Technische Universität München, Lehrstuhl für Entwicklungsgenetik c/o Helmholtz Zentrum München, Munich, Germany.

[14]These authors contributed equally: Gesine Behrens, Stephanie L. Edelmann, Timsse Raj.

Abstract

Roquin and Regnase-1 proteins bind and post-transcriptionally regulate proinflammatory target messenger RNAs to maintain immune homeostasis. Either the *sanroque* mutation in Roquin-1 or loss of Regnase-1 cause systemic lupus erythematosus-like phenotypes. Analyzing mice with T cells that lack expression of Roquin-1, its paralog Roquin-2 and Regnase-1 proteins, we detect overlapping or unique phenotypes by comparing individual and combined inactivation. These comprised spontaneous activation, metabolic reprogramming and persistence of T cells leading to autoimmunity. Here, we define an interaction surface in Roquin-1 for binding to Regnase-1 that included the *sanroque* residue. Mutations in Roquin-1 impairing this interaction and cooperative regulation of targets induced T follicular helper cells, germinal center B cells and autoantibody formation. These mutations also improved the functionality of tumor-specific T cells by promoting their accumulation in the tumor and reducing expression of exhaustion markers. Our data reveal the physical interaction of Roquin-1 with Regnase-1 as a hub to control self-reactivity and effector functions in immune cell therapies.

Post-transcriptional control of mRNA stability or translation through RNA-binding proteins (RBPs) represents an important level of gene regulation with crucial impact on immune cell fate decisions. This role becomes evident from combined genetic inactivation of alleles encoding for the Roquin-1 and Roquin-2 proteins with redundant functions in mice or in a human patient who developed a severe hyperinflammatory syndrome due to a homozygous nonsense mutation in the *RC3H1* gene encoding ROQUIN-1 (refs. [1-3]). Moreover, a single amino acid exchange (M199R), called *sanroque* mutation, in the murine Roquin-1 protein causes lupus-like autoimmunity. Regnase-1-deficient mice exhibit a comparable autoimmune phenotype with activated $CD4^+$ and $CD8^+$ T cells, accumulation of plasma cells, hypergammaglobulinemia and autoantibody production[4,5]. In response to T cell activation, Roquin-1, its paralog Roquin-2 and Regnase-1 are similarly regulated by MALT1-dependent proteolytic cleavage[5,6]. All three RBPs share a number of mRNA targets[3,5-7], suggesting potential cooperation[6,8]. Roquin-1/2 proteins repress the expression of Regnase-1 (refs. [6,8]). Mapping of binding sites of overexpressed Regnase-1 crosslinked to cellular mRNAs revealed the sequence determinants of Roquin-recognized stem loops of the constitutive decay element (CDE)[7,9]. Despite an extensive overlap in phenotypes and regulation of these RBPs, they have different functions. Roquin-1 interacts with

components of the mRNA deadenylation and decapping machinery[9-11], whereas Regnase-1 endonuclease cleaves target mRNAs[4,7,12]. Because Roquin-1 and Regnase-1 were found enriched in P bodies and at the endoplasmic reticulum (ER), respectively and differed in their requirements for regulation of reporter mRNAs, it was proposed that Roquin-1/2 and Regnase-1 proteins function in a compartmentalized manner independently of each other[7,13].

Owing to the prominent humoral autoimmunity occurring in mice with the *sanroque* mutation or Regnase-1 inactivation[4,14] and recapitulation of hallmark phenotypes by T cell-specific deletion of Roquin-1/2 or Regnase-1 (refs.[3,5]), previous studies mostly focused on $CD4^+$ helper T cells. Nevertheless, the ubiquitous expression of Roquin-1/2 and the prevalence of individual Regnase-1/2/3/4 paralogs suggest an importance of both RBP families in many types of cells and fate decisions[15-17]. More recently, inactivation of Regnase-1 in tumor-specific $CD8^+$ T cells or chimeric antigen receptor (CAR)-T cells resulted in increased antitumor responses[18,19], whereas an involvement of Roquin paralogs in $CD8^+$ effector T cell responses has not yet been studied. In the context of defining tumor antigen-specific T cell antigen receptors (TCRs) or CARs, current efforts also try to modulate tumor-specific T cells. The aim is to bolster activation, prevent regulatory T (T_{reg}) cell-induced suppression, reprogram metabolism or break tumor-imposed exhaustion and make adoptive cell therapies (ACTs) efficient for different blood cancers as well as solid tumors.

Here we explore how the interaction of Roquin-1 with Regnase-1 affects peripheral tolerance and how this program can be used in ACT. We show that both proteins bind to each other in a ternary complex on RNA. This interaction was important for the regulation of shared targets and controlled $CD4^+$ and $CD8^+$ T cell quiescence, metabolic programs, T cell activation, differentiation and effector functions. Weakening the physical interaction of Roquin-1 with Regnase-1 by introducing mutations into the mouse germline caused humoral autoimmunity but led to enhanced responses of cytotoxic T cells directed toward tumor-expressed antigens in the tumor setting.

Results

Roquin-1/2 and Regnase-1 maintain quiescence of T cells.

To address the functional relationship of Roquin-1/2 and Regnase-1 proteins we analyzed mice with T cell-specific deletion of the genes encoding Regnase-1 (ref. [20]) (*Zc3h12a*$^{fl/fl}$;*Cd4*-Cre, termed KO^T), Roquin-1 and Roquin-2 (refs. [3,21]) (*Rc3h1*$^{fl/fl}$;*Rc3h2*$^{fl/fl}$;*Cd4*-Cre, termed DKO^T) or a combination of all three genes (*Zc3h12a*$^{fl/fl}$;*Rc3h1*$^{fl/fl}$;*Rc3h2*$^{fl/fl}$;*Cd4*-Cre, termed TKO^T). $CD4^+$ and $CD8^+$ T cells from all mutant mice showed a spontaneous reduction of naive T cells ($CD62L^+CD44^{lo}$) and an increase in effector memory T cells ($CD62L^-CD44^{hi}$) (Fig. 1a,b). Accumulation of effector $CD4^+$ and $CD8^+$ T cells was not due to a reduction in T_{reg} cells, which instead increased in frequencies in all knockout mice and also in numbers in KO^T and TKO^T mice (Fig. 1c,d). Reconstituting lethally irradiated CD45.1/2 congenic mice with mixtures of wild-type (CD45.1) and TKO^T (CD45.2) bone marrow (Extended Data Fig. 1a) revealed that the increase in peripheral T_{reg} cells (Fig. 1c,d) was not cell intrinsic, as we found comparable frequencies of wild-type and TKO^T T_{reg} cells in mixed-bone-marrow chimeric

mice that were increased compared to wild-type/wild-type chimeric mice (Extended Data Fig. 1b). The increased T_{reg} cell frequencies in TKO^T but also KO^T and DKO^T mice presumably occurred secondary to tissue inflammation[3,5,6,22], consistent with the observed infiltration of leukocytes into the lung of mutant mice (Extended Data Fig. 1c). We then asked whether the observed activation of conventional $CD4^+$ and $CD8^+$ T cells also occurred in the presence of wild-type T_{reg} cells. We therefore generated mice in which deletion of Roquin-1/2- and Regnase-1-encoding genes, individually or in combination, can be induced by tamoxifen treatment using the Cre-ERt2 transgene[23]. We adoptively transferred $CD3^+$ T cells (CD45.2) from iKO (*Zc3h12a*$^{fl/fl}$;Cre-ERt2), iDKO (*Rc3h1/2*$^{fl/fl}$;Cre-ERt2) or iTKO (*Rc3h1/2*$^{fl/fl}$;*Zc3h12a*$^{fl/fl}$;Cre-ERt2) mice into congenic (CD45.1) wild-type hosts that were then treated with tamoxifen to acutely delete Roquin-1/2- and Regnase-1-encoding alleles (Fig. 1e). $CD45.2^+$ T cells on day 8 after transfer showed increased frequencies of $CD4^+$ and $CD8^+$ T cells for all knockouts (Fig. 1f). We determined a breakdown of quiescence in knockout $CD4^+$ and $CD8^+$ T cells by increased effector-memory phenotypes (Extended Data Fig. 1d) and enhanced proliferation of these cells indicated by Ki67 staining (Fig. 1g and Extended Data Fig. 1e). These effects were observed in all knockouts but were typically more pronounced upon combined inactivation of Roquin-1/2 and Regnase-1 iTKO T cells. We employed extracellular flux (Seahorse) analyses to determine metabolic reprogramming, a hallmark of T cell activation and functional adaptation, addressing whether inactivation of the different RBPs alters metabolic pathways. During restimulation of $CD4^+$ T cells after in vitro deletion by 4′-OH-tamoxifen treatment we found increased glycolytic activities in all three knockouts compared to wild-type T cells, even under glucose-deprived conditions at baseline. Extracellular acidification rates (ECARs) were even more elevated upon glucose addition and glycolytic capacities were higher in all three knockouts, with the strongest effects in iTKO T cells (Fig. 1h and Extended Data Fig. 2a-c). Mitochondrial respiration was also affected by Roquin-1/2 and Regnase-1 deficiencies and, at baseline, oxygen consumption rates (OCRs) were elevated in all knockouts with a highest increase in iTKO T cells. OCR changes were more pronounced than ECARs suggesting that knockout T cells fuel their energetic demands to a main extent from OXPHOS (Fig. 1h and Extended Data Fig. 2d,e). Consecutively, maximal respiration rates and respiratory spare capacities were increased in all knockout genotypes but were highest in iTKO T cells (Extended Data Fig. 2d,e). With regard to mitochondrial respiration, Regnase-1 deficiency contributed stronger to the deregulation of metabolism compared to Roquin-1/2 deficiency. Similar metabolic reprogramming was also observed for knockout $CD8^+$ T cell cultures; however, $iTKO^T$ $CD8^+$ T cells showed variable effects in glycolytic tests, especially in mitochondrial stress tests (Extended Data Fig. 2f,g and Supplementary Table 1). These data show that Roquin-1/2 and Regnase-1 inactivation leads to a general metabolic reprogramming with increased energy generation from mitochondrial respiration and enhanced glycolytic capacity.

Roquin-1/2 and Regnase-1 control humoral autoimmunity.

Cd4-Cre mediated deletion of Roquin-1/2 encoding alleles has been associated with follicular helper T (T_{FH}) cell (PD-1^{hi}Cxcr5^{hi}, $Bcl6^+$) accumulation[3], which we also detected in KO^T and even stronger in TKO^T mice (Fig. 2a). In addition, all mutant mice showed an accumulation of germinal center (GC) B cells ($GL7^+CD95^+$) (Fig. 2b). We combined floxed alleles with an inducible *Cd4*-Cre-ERt2 knock in allele[24,25] and adoptively transferred

naive $CD4^+$ T cells ($CD45.2^+$) from wild-type, iKO, iDKO and iTKO mice into congenic ($CD45.1^+$) wild-type mice that were then treated with tamoxifen (Fig. 2c and Extended Data Fig. 2h). Knockout $CD4^+$ T cells spontaneously differentiated into T_{FH} cells in vivo 6 d after acute gene deletion (Fig. 2d,e). Different from non-inducible deletion, the inducible inactivation of Regnase-1 (iKO^T) showed strongest T_{FH} cell accumulation compared to iTKO and iDKO, suggesting an advantage of this genotype in the adoptive transfer. Indeed, at a late time point, 7 weeks after transfer, we observed significantly increased numbers of iKO T cells compared to wild-type and iDKO T cells, which also occurred, albeit to a lesser extent, in iTKO T cells (Fig. 2f). Considering intermediate frequencies of dividing iKO $CD4^+$ T cells compared to iDKO and iTKO genotypes early after transfer (Fig. 1f), this finding suggested that Regnase-1 deficiency promotes survival of T cells. Associated with their increased persistence, iKO T cells were capable of inducing autoimmunity in wild-type host mice within 7 weeks (Fig. 2g,h). Transfer of iKO T cells into congenic hosts resulted in accumulation of GC B cells and plasma cells (Fig. 2g and Extended Data Fig. 2i,j) and induced anti-nuclear antibodies (ANAs) in the serum of recipient mice (Fig. 2h). This phenotype was consistent with the appearance of autoantibodies in the serum of 6–8-week-old KO^T and TKO^T (but not DKO^T) mice (Fig. 2i and Supplementary Table 1). Together, these data demonstrate that the autoimmunity associated with the absence of Roquin-1/2 and Regnase-1 genes is caused by deviation of helper T cell functions, because autoimmunity can be transferred with $CD4^+$ T cells, develops in the presence of wild-type T_{reg} cells and originates from a normal T cell receptor repertoire.

Roquin-1/2 and Regnase-1 control $CD8^+$ T cell functions.

CRISPR–Cas9-mediated inactivation of Regnase-1 yielded in improved antitumor responses of adoptively transferred $CD8^+$ or CAR-T cells[18,19]. We therefore analyzed $CD8^+$ T cell phenotypes after conditional deletion of the different RBPs by *Cd4*-Cre-mediated deletion (Fig. 3 and Extended Data Fig. 3). The majority of Roquin-1/2-deficient DKO^T $CD8^+$ T cells adopted a short-lived effector cell (SLEC) phenotype with upregulated KLRG1 (Fig. 3a,b) and downregulated TCF-1 expression (Fig. 3c,d). Fewer Regnase-1-deficient (KO^T) $CD8^+$ T cells showed increased KLRG1 expression with a majority of cells maintaining high TCF-1 expression (Fig. 3a-d). This finding is consistent with a previous report on retained TCF-1 expression after CRISPR–Cas9-mediated inactivation of Regnase-1 in CAR-T cells[19]. Notably, the TKO^T genotype was similar to either Regnase-1 or Roquin-1/2-deficiencies as it moderately increased KLRG1 and strongly reduced TCF-1 expression (Fig. 3a-d). Analyzing additional markers of activation, stemness and exhaustion[26,27] (Extended Data Fig. 3a) we found increased expression of ICOS, CTLA-4 and CD38 in all knockouts. Regnase-1 deficiency increased CXCR5, whereas Roquin-1/2 deficiency induced PD-1 and Tim3 expression (Extended Data Fig. 3a). All knockout T cells showed elevated expression of the transcription factor BATF (Extended Data Fig. 3b), as reported before for inactivation of Regnase-1 (ref. [18]). $CD8^+$ T cells from all genotypes showed the capacity to produce tumor necrosis factor (TNF) upon ex vivo stimulation, but only knockout T cells simultaneously produced TNF and interferon (IFN)-γ (Fig. 3e and Extended Data Fig. 3c). Only $CD8^+$ T cells with Regnase-1 deficiency (KO^T or TKO^T) acquired an enhanced ability to produce interleukin (IL)-2 (Fig. 3f and Extended Data Fig. 3d), whereas all knockout T cells had increased granzyme B expression compared to wild-type counterparts (Fig. 3g

and Extended Data Fig. 3e). To quantify cytotoxicity in vitro, we redirected polyclonal $CD8^+$ T cells toward P815 mastocytoma tumor cells in the presence of anti-CD3 (Fig. 3h). All knockout T cells showed enhanced killing in a chromium-release assay, but we observed strongest effects for Roquin-1/2 (DKO^T) compared to Regnase-1 deficiencies (KO^T) and intermediate effects were seen for TKO^T $CD8^+$ T cells. We then addressed whether inactivation of Roquin-1/2 or Regnase-1 leads to increased $CD8^+$ effector responses in a B16-OVA melanoma model by adoptively transferring $CD8^+$ TCR-transgenic OT-I T cells into hosts that had received tumor cells 3 d before (Fig. 3i). Of note, hosts that received PBS or wild-type OT-I T cells showed exponential tumor growth between days 7–21, whereas either Regnase-1 or Roquin-1/2-deficient OT-I T cells suppressed tumor formation resulting in delayed occurrence of measurable tumors and reduced affection rates of recipient mice (Fig. 3j). Together these data show that Roquin-1/2 and Regnase-1 proteins also control shared cellular programs in cytotoxic T cells, but both RBPs have different contributions to the individual phenotypes (Supplementary Table 1).

Roquin-1 and Regnase-1 exhibit functional interaction.

To address post-transcriptional interaction, we tested the contribution of Roquin-1/2 and Regnase-1 to the regulation of ICOS, a well-described target of these RBPs[3,5,10,28]. We performed tamoxifen gavage of mice to acutely delete floxed alleles by *Cd4*-Cre-ERt2 in vivo. Isolated naive $CD4^+$ T cells were stimulated in vitro for 2 d with anti-CD3/CD28 under type 1 helper T (T_H1) cell conditions, as ICOS expression differs among helper T cell subsets[10,29]. Appropriate deletion was confirmed in immunoblots (Fig. 4a). In wild-type T cells Roquin-1, the much lower-expressed Roquin-2, as well as Regnase-1 proteins increased during days 1–2 and consistent with TCR-induced MALT1 activity, accumulated as cleavage products. Upon removal of TCR stimulation (days 3–5) the full-length Roquin-1/2 and Regnase-1 proteins increased and the cleavage product of Regnase-1 disappeared. By contrast, cleaved Roquin-1 persisted, suggesting either a longer half-life or constitutive cleavage of this protein (Fig. 4a). Consistent with the Regnase-1-encoding *Zc3h12a* mRNA being a target of Roquin-1/2 (ref. [6]), the Regnase-1 protein became strongly induced in iDKO T cells, whereas Roquin-1/2 expression was unchanged upon Regnase-1 inactivation (Fig. 4a), in contrast to results obtained in a human T cell line[22]. ICOS protein expression on wild-type T_H1 cells increased during stimulation (days 1–2) and returned to basal expression after stimulation (days 3–5). In iTKO compared to wild-type T cells, ICOS protein expression was strongly de-repressed at all time points starting at the naive stage (day 0) (Fig. 4b). Notably, iTKO cells were almost unable to decrease ICOS protein expression after removal of the TCR stimulus (days 3–5) (Fig. 4b). Inactivation of either Roquin-1/2 (iDKO) or Regnase-1 (iKO) increased ICOS protein expression during (day 1–2) and after stimulation (days 3–5) intermediate to wild-type and iTKO T_H1 cells. Different from the iTKO genotype, iDKO and iKO T_H1 cells were partially able to decrease ICOS protein after stimulation (Fig. 4b). We then tested whether Roquin-1 and Regnase-1 can complement in the absence of each other and whether redundancy existed among Regnase paralogs (Fig. 4c). To address these questions, we reconstituted Regnase-1 (iKO)- or Roquin-1/2 (iDKO)-deficient $CD4^+$ T cells with doxycycline-inducible, green fluorescent protein (GFP)-tagged Roquin-1 or Regnase-1, Regnase-2, Regnase-3 and Regnase-4 proteins (Extended Data Fig. 4a). In these assays we quantified endogenous ICOS and Regnase-1

expression on day 4 of T cell activation. Notably, exogenous GFP–roquin-1 was readily able to decrease Regnase-1 or ICOS expression in iDKO T cells, but was only partially able to downregulate ICOS expression in Regnase-1-deficient (iKO) T cells (Fig. 4c). Endogenous Regnase-1 protein displays strong regulation of *Zc3h12a* mRNA by Roquin and Regnase-1 (Fig. 4a and refs. [6,30]). To distinguish endogenous from overexpressed Regnase-1 protein, we altered the epitope within GFP–regnase-1 that is recognized by the monoclonal antibody used for detection (Extended Data Fig. 4b,c). While becoming invisible to the antibody, GFP–regnase-1^{invis} protein remained fully able to downregulate targets such as CTLA-4 (Extended Data Fig. 4d). The analysis of iKO T cells reconstituted with ectopic Regnase-1^{invis}, Regnase-2, Regnase-3 or Regnase-4 revealed that all four Regnase paralogs were able to downregulate ICOS expression in the absence of endogenous Regnase-1, with only Regnase-4 being slightly less efficient (Fig. 4c and Extended Data Fig. 4e). Ectopic expression of the same Regnase paralogs in Roquin-1/2-deficient T cells showed that neither Regnase-1^{invis} nor Regnase-2, Regnase-3 or Regnase-4 were able to efficiently downregulate endogenous ICOS or Regnase-1 protein expression (Fig. 4c and Extended Data Fig. 4f). Therefore, full regulation of these shared targets required Roquin-1/2 and Regnase-1 proteins.

Molecular determinants of Roquin cooperation with Regnase-1.

To better understand the functional interaction in the regulation of mRNA targets by Roquin and Regnase-1, we searched for a minimal region in Roquin-1 that was able to regulate shared targets. Notably, in iDKO T cells the amino-terminal MALT1 cleavage product of Roquin-1 (Roquin-1$^{aa1\text{-}510}$) showed partial or almost full activity to downregulate ICOS or Regnase-1 expression, respectively, but was unable to repress Ox40 (*Tnfrsf4*), another well-known target[3,5,31] (Extended Data Fig. 5a-c). This truncated version of Roquin-1 exerted a slight dominant–negative effect on Regnase-1 and Ox40 protein expression when we induced its expression in wild-type T cells (Extended Data Fig. 5d). Deletion analyses indicated that the core RNA-binding domain of Roquin-1 containing $HEPN_N$/ROQ/$HEPN_C$ was sufficient to suppress Regnase-1 expression in iDKO T cells (Extended Data Fig. 5e). We then utilized the interdependent regulation of endogenous Regnase-1 as a readout to screen a set of Roquin-1 point mutants. We exchanged residues on the surface of the $HEPN_N$/ROQ/$HEPN_C$ domains of Roquin-1 with mutations that alter physical properties but were predicted not to interfere with folding (Extended Data Fig. 6a) and found residues M199, E201, E202, L209, E212, D213, L217, F225, D322 in the ROQ domain essential for Roquin-1$^{aa1\text{-}510}$-mediated repression of Regnase-1 (Fig. 4d). Projecting these residues onto the ROQ domain structure[32-34] revealed a site of potential interaction between Roquin-1 and Regnase-1 that is different from the RNA interaction surface (Fig. 4e). Notably, amino acid M199 of Roquin-1, which is mutated in *sanroque* mice, is part of this patch of residues in the ROQ domain (Fig. 4e) and overexpression of this mutant in wild-type T cells did not exhibit a dominant–negative effect on Regnase-1 or ICOS expression (Fig. 4f and Extended Data Fig. 6b). Instead, M199R, L209Y and E212K Roquin-1 mutants in the full-length protein were impaired to downregulate ICOS and Regnase-1 in iDKO T cells at the protein and mRNA level (Fig. 4g and Extended Data Fig. 6c,d). However, all mutants were fully active to repress Ox40 (Fig. 4g and Extended Data Fig. 6c,d) and, similar to wild-type GFP–roquin-1 protein, localized to P bodies, as identified by the RNA helicase Rck, a marker of

P bodies[10] (Extended Data Fig. 6e). The *sanroque* mutation (M199R) as well as the newly identified L209Y and E212K mutants therefore create hypomorphic Roquin-1 variants that have impaired co-regulation activity with Regnase-1 of ICOS and Regnase-1-encoding target mRNAs. These mutations did not affect Ox40 regulation, consistent with regulation of this target mRNA being fully dependent on the carboxy terminus of Roquin-1 and its interaction with the CCR4-NOT complex[2]. These data demonstrate that shared mRNA targets can be subject to full (*Zc3h12a*) or partial cooperation (*Icos*) as well as independent (*Tnfrsf4*) modes of regulation by Roquin-1 and Regnase-1.

Roquin and Regnase-1 form a ternary complex on RNA.

To determine whether post-transcriptional co-regulation can be explained by direct interaction of Roquin-1 with Regnase-1, we performed co-immunoprecipitation and Förster Resonance Energy Transfer (FRET) experiments. Roquin-1 could be co-immunoprecipitated with Regnase-1 from lysates of wild-type but not iKO $CD4^+$ T cells (Extended Data Fig. 7a). To obtain spatial information on this interaction in living cells, we used fluorescence lifetime imaging (FLIM) in HeLa cells co-transfected with GFP–regnase-1 and mCherry–roquin-1. In these experiments the reduction of fluorescence lifetime of GFP is caused upon energy transfer from GFP to mCherry and can be used to quantify donor–acceptor interactions. Both fluorescent proteins localized diffusely in the cytoplasm and colocalized with the P-body marker Rck tagged by blue fluorescent protein (BFP) (Fig. 5a). We found enrichment of GFP–regnase-1 at the ER as reported earlier[7], but only in cells that were not co-transfected with Roquin-1 (Extended Data Fig. 7b). Moreover, sucrose gradient centrifugation of T cell extracts showed the majority of endogenous Regnase-1 co-migrating with Roquin-1 in fractions without monosomes or polysomes (Extended Data Fig. 7c). Notably, GFP–regnase-1 interacted with mCherry–roquin-1 as evidenced by the reduced fluorescence lifetime of GFP in the presence of mCherry–roquin-1 (Fig. 5a,c) but not in its absence (Fig. 5b,c). This energy transfer occurred mainly in P bodies but also dispersed in the cytoplasm. Expression of mCherry–roquin-$1^{aa1\text{-}510}$ also reduced the lifetime of GFP–regnase-1 fluorescence, albeit to a lesser extent (Fig. 5c), confirming that the amino terminus of Roquin-1 is sufficient for the interaction. As all four Regnase paralogs were able to downregulate ICOS expression in Regnase-1-deficient iKO T cells (Fig. 4c), we tested the PIN domain of Regnase-1, which is highly conserved among Regnase paralogs[35]. The truncated GFP–regnase-$1^{aa112\text{-}297}$ protein was localized to the cytoplasm and nucleus and, similar to truncated Roquin-$1^{aa1\text{-}510}$, was no longer enriched in P bodies (Extended Data Fig. 7d,e). The truncated form of GFP–regnase-$1^{aa112\text{-}297}$ also exhibited a reduction in fluorescence lifetime mainly in the cytoplasm where it colocalized with mCherry–roquin-$1^{aa1\text{-}510}$ (Extended Data Fig. 7d,e).

To finely map the structural details of this interaction, we introduced the identified mutations (Fig. 4d,g) in NanoLuc–roquin-$1^{aa1\text{-}510}$ fusion proteins and coexpressed them with HaloTag–regnase-1 to perform NanoBRET assays (Fig. 5d). Co-transfected cells were analyzed for energy transfer from nano-luciferase to the HaloTag ligand. We observed a similar BRET signal for wild-type Regnase-1 and Roquin-1 proteins as for the positive controls (p53 and MDM2). Of note, single ROQ domain mutants of Roquin-1 (M199R, L209Y and E212K) as well as double mutants (M199R/L209Y or M199R/E212K)

effectively reduced the BRET signal. Mutations that interfere with Roquin-1 binding to RNA (K220A/K239A/R260A) (ref. [32]) did not reduce the interaction with Regnase-1. To confirm direct protein–protein interaction, we used surface plasmon resonance (SPR) with purified recombinant proteins. By immobilizing Roquin-1$^{aa2\text{-}440}$ on the surface of a Biacore chip and adding Regnase-1$^{aa1\text{-}452}$ protein in solution, we demonstrated formation of a stable binary Roquin-1 and Regnase-1-containing complex at nanomolar affinity (K_D = 417 nM) (Fig. 5e). Next, we used a pulldown assay to quantify how the identified mutations in Roquin-1 affect direct binding of recombinant proteins. A larger, SUMO-tagged wild-type Roquin-1 protein was mixed with a shorter (untagged) version of Roquin-1 harboring different mutations. We quantified the ability of both proteins to compete for interaction with immobilized, GST-fused Regnase-1 full-length protein (Fig. 5f). The ratio of Regnase-1 bound untagged Roquin-1 mutants to the SUMO-tagged wild-type Roquin-1 proteins in these pulldown experiments revealed three- to fourfold weaker interactions for M199R/L209Y or M199R/E212K Roquin-1 mutants (Fig. 5f and Extended Data Fig. 7f). Of note, single M199R, L209Y or E212K mutants only resulted in a twofold reduction of binding (Extended Data Fig. 7g, h). We next analyzed the interaction of Roquin-1 and Regnase-1 in RNA-electrophoretic mobility shift assays (EMSAs). We used the RNA-binding sufficient amino terminus of Roquin-1$^{aa2\text{-}440}$ and the RNase-dead version Regnase-1$^{aa1\text{-}452;\ D141N}$ to avoid RNA degradation[4] and asked whether these proteins can form a ternary complex with the 3′-UTR stem loop of the *Zc3h12a* mRNA (nt194–212) (ref. [30]) (Fig. 5g). Indeed, the stem loop of the *Zc3h12a* mRNA was specifically bound by Roquin-1$^{aa2\text{-}440}$ and increasing Regnase-1 concentrations in these binding reactions decreased the Roquin-specific band and induced a supershift (Fig. 5g). Collectively, these data establish Roquin-dependent recognition of the mRNA stem loop and additional interactions of the RNA-bound Roquin-1 protein with Regnase-1.

Roquin-1 interaction with Regnase-1 prevents autoimmunity.

We then addressed the functional consequences of interfering with Roquin-1 and Regnase-1 interaction in vivo. We introduced two different *Rc3h1* mutations encoding for Roquin-1 L209Y or E212K, exhibiting weaker or stronger inhibition of interaction and cooperative regulation with Regnase-1, into the mouse germline. Homozygous mice expressing *Rc3h1* mutations encoding for E212K, L209Y or M199R increased the frequencies of activated CD44$^+$CD4$^+$ T cells (Fig. 6a,b), increased T cell proliferation (Fig. 6c,d), caused a T_H1 cell bias with increased IFN-γ production of ex vivo-stimulated CD4$^+$ T cells (Fig. 6e,f and refs. [22,36]) and also induced accumulation of effector memory CD8$^+$ T cells compared to wild-type mice, which was strongest for E212K mutant (Fig. 6g,h). E212K mutant mice showed compromised viability so that only two homozygous animals could be analyzed to date. Together, these data suggest that Roquin-1$^{L209Y/L209Y}$ or Roquin-1$^{E212K/E212K}$ expressing mice phenocopy the *sanroque* phenotype.

We then addressed whether the *sanroque* phenotype[14] develops only due to altered T cell functions. As heterozygosity of the *sanroque* allele has no phenotype in young mice[37], we combined one *Rc3h1*^{san} and one *Rc3h1*^{fl} allele with *Cd4*-Cre or Vav-Cre. This allowed us to compare phenotypes of the *sanroque* allele originating from T lymphocytes versus hematopoietic cells (Fig. 6i-k and Extended Data Fig. 8a-c). Vav-Cre-mediated deletion

of the floxed *Rc3h1* allele was much more potent to induce T cell activation (Fig. 6i and Extended Data Fig. 8a) and GC B cell accumulation compared to *Cd4*-Cre (Fig. 6k and Extended Data Fig. 8c), whereas T_{FH} cell differentiation was similarly increased for both Cre lines (Fig. 6j and Extended Data Fig. 8b). This result indicated T cell-extrinsic contributions of the *sanroque* allele to the observed activation of T cells and accumulation of GC B cells.

Similar to the *sanroque* allele, heterozygosity of alleles encoding L209Y/+ or E212K/+ did not induce obvious phenotypes in young mice (Fig. 7). To formally test whether L209Y and E212K induce the same functional impairment in Roquin-1 as the M199R-encoding allele, we generated mice encoding two heterozygous mutations and compared their phenotypes to mice with homozygous M199R-encoding or wild-type alleles. $CD4^+$ T cells from mice carrying mutations encoding Roquin-$1^{M199R/L209Y}$ and Roquin-$1^{M199R/E212K}$ showed a pronounced increase in frequencies of effector memory (Fig. 7a,b) and T_{FH} cells (Fig. 7c,d) compared to wild-type or heterozygous mutant mice with one wild-type allele (Fig. 7a-d). The heterozygous combination with one *sanroque* allele also caused spontaneous formation of germinal centers in the majority of B cell follicles of the spleen (Fig. 7e) and induced GC B cells in the absence of immunization (Fig. 7f,g). Analyzing autoantibodies in the sera of mice at 8–12 weeks of age (Fig. 7h) we found that homozygous *sanroque* mice expressing Roquin-$1^{M199R/M199R}$, different from heterozygous Roquin-$1^{M199R/+}$ mice, showed a wide range of elevated titers of ANAs, which were partially matched by mice expressing the compound Roquin-$1^{M199/E212K}$, Roquin-$1^{L209Y/L209Y}$ and Roquin-$1^{E212K/E212K}$. In fact, mice expressing Roquin-$1^{M199R/E212K}$ showed significantly increased titers of ANAs when compared to mice expressing Roquin-$1^{M199R/+}$. Collectively, our data demonstrate that the Roquin-1 L209Y and E212K mutants induce phenotypes similar to *sanroque* mice. Notably, the heterozygous combination of E212K- and M199R-encoding alleles revealed compound effects and autoimmunity equivalent to homozygous *sanroque* mice expressing the Roquin-1^{M199R} protein.

Roquin-1 interaction with Regnase-1 inhibits antitumor immunity.

Based on our previous findings demonstrating enhanced cytotoxic activities of Regnase-1 or Roquin-1/2-deficient $CD8^+$ T cells, we asked whether the mixed heterozygous Roquin-$1^{M199R/E212K}$ or *sanroque* mouse mutants that showed elevated autoantibody titers would also exhibit enhanced antitumor responses. First, we established that OT-I $CD8^+$ T cells from heterozygous *sanroque* mice (Roquin-$1^{M199R/+}$) were not effective in conferring protection from tumor growth in the B16-OVA model, as they were comparable to $CD8^+$ T cells from OT-I wild-type mice (Fig. 8a). In the OT-I context we determined only a moderately increased effector memory phenotype in T cells expressing Roquin-$1^{M199R/E212K}$ or Roquin-$1^{M199R/M199R}$ proteins (Fig. 8b). Nevertheless, mice receiving OT-I T cells with either of the two mutations were largely protected from tumor growth as compared to control-treated tumor bearing mice (Fig. 8c). Similar to previous observations on Regnase-1 inactivation[18], the frequency of transferred OT-I TCR-transgenic relative to endogenous $CD8^+$ T cells increased more in the tumor than in the spleen for T cells with mutations encoding Roquin-$1^{M199R/E212K}$ or Roquin-$1^{M199R/M199R}$ (Fig. 8d) and these mutant OT-I T cells showed similar upregulation of CD44 but moderately increased

KLRG1 expression compared to wild-type OT-I T cells (Fig. 8e). Of note, analyzing PD-1 or TOX as markers of exhaustion[38] revealed decreased expression on T cells of mice expressing Roquin-1$^{M199R/E212K}$ or Roquin-1$^{M199R/M199R}$ (Fig. 8f-i). Moreover, CD101, which marks terminally exhausted CD8$^+$ T cells in chronic infections[26], was strongly expressed on wild-type OT-I T cells in the tumor, but almost absent from OT-I T cells expressing Roquin-1$^{M199R/E212K}$ or Roquin-1$^{M199R/M199R}$ proteins. Together, these data show that inhibition of Roquin-1 interaction with Regnase-1 promotes the effector function of tumor-specific T cells by increasing their abundance and attenuating their functional inactivation in the tumor.

Discussion

We describe the direct physical interaction of Roquin-1 and Regnase-1 proteins on RNA. Our findings reveal cooperative regulation of *Icos* and *Zc3h12a* (Regnase-1) mRNAs within the shared target set[7,9,39-41] and explain overlapping phenotypes of Roquin-1/2 and Regnase-1 mutant mice[3,5,14]. Conditional inactivation of Roquin-1/2 or Regnase-1 in T cells or germline mutations introducing M199R (*sanroque*), L209Y and E212K substitutions in the ROQ domain of Roquin-1 that similarly interfere with Roquin-1 binding to Regnase-1, caused autoimmunity. This role in peripheral tolerance becomes evident from spontaneous activation of T cells and accumulation of T_{FH} cells and GC B cells in all mouse lines, as well as autoantibody formation in some mouse lines.

Analyzing similar changes induced through acute deletion of RBP-encoding alleles in T cells, we find that the Roquin-1/2 and Regnase-1 proteins are continuously required in naive T cells to maintain quiescence. These proteins silence cell-intrinsic programs of activation and proliferation associated with metabolic reprogramming to increased glycolysis and enhanced oxidative phosphorylation. Although both Roquin-1/2 and Regnase-1 proteins have already been found to be negative regulators of the mTOR pathway, protein biosynthesis and purine metabolism[42,43], it is currently unclear which target(s) are driving the observed metabolic changes and trigger spontaneous activation of T cells. Following activation, CD4$^+$ T cells committed to the T_{FH} cell subset and CD8$^+$ T cells acquired polyfunctionality and enhanced cytotoxic activity. In our phenotypic comparisons, contributions from Roquin-1/2 and Regnase-1 were often comparable and combined inactivation typically showed increased effects. The related phenotypes indicate that these RBPs cooperate in the same pathways. Cooperative post-transcriptional regulation can either be explained by binding in a complex to the same mRNA, as established here. It can also be explained by independent binding of the different RBPs to the same mRNA[44] or independent binding to different molecules of the same mRNA species as suggested previously[7,13,22] or independent binding to different mRNA species that then cooperate in the same pathway. Understanding how cooperation is encoded in the transcripts of *Icos* and *Zc3h12a* but not in *Tnfrsf4* and thereby allows formation of differential messenger ribonucleoproteins will require extensive structural, biochemical and functional analyses. Of note, our data also revealed selective contributions, especially for CD8$^+$ T cells. Regnase-1 deficiency was associated with increased persistence of CD4$^+$ and CD8$^+$ T cells[5,18] and enabled CD8$^+$ T cells to produce copious amounts of IL-2. By contrast, Roquin-1/2 deficiency induced KLRG1 expression in CD8$^+$ T cells, caused downregulation of TCF-1

and strongly increased in vitro cytotoxicity. Nevertheless, inactivation of either Roquin-1/2 or Regnase-1 improved antitumor responses and a comparable improvement resulted from interfering with Roquin-1–Regnase-1 interaction.

Here, we present the interaction of Roquin-1 with Regnase-1 as a molecular mechanism underlying the prevention of autoimmunity and propose that this interaction can become a promising target for improvement of therapeutic approaches with adoptively transferred antigen-specific T cells.

Methods

Mice.

All mice used in this study were on a C57BL/6 background. All animals were housed in a specific-pathogen-free barrier facility under a 12 h/12 h dark/light regime at 20–24 °C and at a humidity of 45–65% in accordance with the Helmholtz Zentrum München and the Ludwig-Maximilians-Universität München institutional, state and federal guidelines. All experimental procedures involving male or female mice were performed in accordance with regulations and were approved by the local government (Regierung von Oberbayern reference nos. 55.2-2532-Vet_02-19-122, 55.2-2532.Vet_02-17-159, 55.2-2532.Vet_02-18-10 and 55.2-2532.Vet_02-19-68). *Rc3h1/2*$^{fl/fl}$ mice are transgenic for the Roquin-1-encoding gene *Rc3h1* (ref. [21]) and the Roquin-2-encoding gene *Rc3h2*[3]. *Zc3h12a*$^{fl/fl}$ mice are transgenic for the Regnase-1-encoding gene *Zc3h12a*[20]. Transgenic *Rc3h1/2*$^{fl/fl}$ mice were crossed to *Zc3h12a*$^{fl/fl}$ mice to reach the final genotype of *Rc3h1/2*$^{fl/fl}$;*Zc3h12a*$^{fl/fl}$, which were crossed with either *Cd4*-Cre[45], Cre-ERt2 (ref. [23]) or *Cd4*-Cre-ERt2 (ref. [24]) transgenic mice. For tumor experiments, OVA-specific transgenic TCR was introduced by crossing mice to the OT-I line[46]. Rc3h1/2$^{fl/fl}$;*Cd4*-cre-ERt2;rtTA-M2 or *Zc3h12a*$^{fl/fl}$;*Cd4*-cre-ERt2;rtTA-M2 mice were generated by crossing mice with respective loxP sites and *Cd4*-cre-ERt2 with Gt(ROSA)26Sortm1(rtTA*M2) Jae mice[47]. The *Rc3h1*^{M199R} mice (*sanroque*) (EM:02168) were obtained from the European Mouse Mutant Archive consortium and mice expressing CD45.1 (*Ptprc*^{a} *Pepc*^{b}/BoyJ), Vav-iCre (Jax no. 00861) as well as Gt(ROSA)26Sortm1(rtTA*M2)Jae mice were obtained from the Jackson Laboratory. Data collection and analysis were not performed blind to the conditions of the experiments. Experimental groups were assigned according to genotype.

Generation of *Rc3h1* mutant mouse lines via CRISPR–Cas9-based gene editing.

The *Rc3h1_E212K* mouse line was generated by Polygene Transgenetics via CRISPR–Cas9 gene editing of the ES cell line and blastocyst injection and the *Rc3h1_L209Y* mouse line via CRISPR–Cas9-based gene editing by electroporation of one-cell embryos. Specific guide RNAs (Rc3h1_L209Y_gRNA: 5′-CAATGCAGAACCATCTTCTA-3′) were used in form of in vitro transcribed single gRNA (EnGen sgRNA Synthesis kit, NEB, E3322). Before electroporation, the specific sgRNA(200 ng μl^{-1}) and single-strand oligonucleotides (ssODN_Rc3h1_L209Y: 5′-TTGTACCATTTTTCCTAGCGATGCAGGAGGAAGCTCTGAAGCTGGTCTTGTATGCTTTAGAAGATGGTTCTGCATTGTCTCGGAAAGTGTTGGTTCTCTTCGTGGTGCAAAGACTGGAGC-3′; 300 ng μl^{-1}) were diluted in Opti-MEM buffer (Thermo Fisher

Scientific) together with recombinant Cas9 protein (200 ng μl^{-1}, IDT) and incubated for 10 min at 20 °C and 10 min at 37 °C to form the active ribonucleoprotein complex. One-cell embryos were obtained by mating C57BL/6N males (Charles River) with C57BL/6N females super-ovulated with 5 U pregnant mare's serum gonadotropin and 5 U human chorionic gonadotropin and electroporated using an NEPA21 electroporator and a CUY501P1-1.5 electrode (Nepa Gene Co). Zygotes were transferred into pseudopregnant CD1 female mice to obtain live pups. Gene-editing events were analyzed on genomic DNA isolated from ear biopsies of founder mice and F1 progeny using the Wizard Genomic DNA Purification kit (Promega, A1120) following the manufacturer's instructions.

Isolation, in vitro cultivation and transduction of primary CD4+ T cells.

Isolation, in vitro deletion of floxed alleles, in vitro cultivation and transduction of primary $CD4^+$ T cells was performed as described[44]. In reconstitution experiments, for induction of pRetro-Xtight-GFP construct expression in rtTA expressing T cells, transduced cells were cultured in the presence of doxycycline (1 $\mu g\ ml^{-1}$) for 16 h before flow cytometry analysis or 6 h before sorting of GFP^+ cells for quantitative PCR with reverse transcription (RT–qPCR).

In vivo deletion of floxed alleles.

Male and female *Cd4*-Cre-ERt2 mice (age 8–16 weeks) with alleles encoding Roquin and Regnase-1 were fed by oral gavage with 5 mg tamoxifen (Sigma) in corn oil per dose on three consecutive days with two doses of tamoxifen on the last day (20 mg total tamoxifen dose per mouse). Mice were killed 3 d after the last gavage and total $CD4^+$ T cells were isolated using the EasySep Mouse T Cell Isolation kit (STEMCELL) according to manufacturers' instructions.

Generation of mixed-bone-marrow chimeric mice.

Bone marrow cells were isolated from femurs and tibias, frozen in FCS containing 10% dimethylsulfoxide and stored at −80 °C until injected into mice. Male and female CD45.1/2 heterozygous recipient mice (age 8–11 weeks) were lethally irradiated with 2 × 5.5 Gy with a XStrahl CIX2 X-ray device. Then, 4×10^6 bone marrow cells were injected intravenously (i.v.) into CD45.1/2 heterozygous recipient mice. Mice were treated for 2 weeks with water supplemented with antibiotics in drinking water (0.04% Baytril) and 9 weeks after irradiation, reconstituted cells were analyzed by flow cytometry.

Adoptive T cell transfer.

Total $CD3^+$ T cells, naive $CD4^+$ T cells or $CD8^+$ T cells were isolated from donor mice using the EasySep Mouse $CD3^+$ Cell Isolation kit, Mouse Naive $CD4^+$ T Cell Isolation kit or Mouse $CD8^+$ Cell Isolation kit (STEMCELL), respectively, according to manufacturers' instructions. Then, 1.5×10^6 cells were injected i.v. into 10-week-old male and female $CD45.1^+$ WT recipient mice. On day 1 and 2 after injection all recipient mice were fed 5 mg tamoxifen by oral gavage twice per day (20 mg total tamoxifen per mouse). Mice were killed on day 8 or day 49 after receiving the first tamoxifen dose.

Ex vivo T cell stimulation.

Total splenocytes were stimulated with 20 nM PMA and 1 μM ionomycin for a total of 4 h. After 1 h of stimulation 10 μg ml^{-1} brefeldin A was added. The reaction was stopped by washing the cells with cold PBS twice before proceeding with antibody staining for flow cytometry.

^{51}Cr-release assay.

Cell-mediated cytotoxicity was determined by a redirected lysis assay. P815 mastocytoma target cells were labeled with 50 μCi ^{51}Cr for 1 h at 37 °C. After washing, 2,000 target cells per 96-well were incubated with effector cells ($CD8^+$ T cells isolated from lymph nodes and spleen) at different effector:target (E:T) ratios in the presence of anti-CD3 (clone (cl.) 145-2C11H, 1 μg ml^{-1}, inhouse production) for 4 h at 37 °C. Subsequently, the amount of radioactivity in the supernatant was measured using a scintillation counter (TopCount NXT).

Melanoma tumor model.

Male and female C57BL/6 wild-type mice were subcutaneously injected with 2×10^5 B16-OVA tumor cells. After 3 d, congenically marked OT-I T cells (1×10^6 i.v.) were adoptively transferred directly after isolation. Tumors were measured manually with a caliper three times per week and tumor size was calculated according to the formula (length × $width^2$) / 2. Mice were humanely killed if the maximal permitted tumor size of 1,400 mm^3 was reached. Otherwise spleens and tumors were collected not later than 21 d after tumor engraftment, cut into small pieces and passed through a 100-μm diameter filter.

Flow cytometry and data analysis with FlowJo.

Single-cell suspensions were stained with fixable blue viability dye (Thermo Fisher Scientific) for 20 min at 4 °C. For the detection of surface proteins cells were stained with the appropriate antibodies in FACS buffer (2% FCS, 1 mM EDTA in PBS) for 20 min at 4 °C. For intracellular staining of cytokines, Roquin, Regnase-1 or CTLA-4 cells were fixed with 2% formaldehyde at 20 °C for 15 min, washed with saponin permeabilization buffer (0.5% saponin and 1% BSA in PBS) and stained with the appropriate antibodies in saponin buffer for 40 min at 4 °C. For commercially available intracellular antibodies, cells were fixed with Foxp3 Fixation/Perm buffer (eBioscience) according to the manufacturer's protocol for 30 min at 4 °C, permeabilized with Foxp3 permeabilization buffer (eBioscience) and stained with antibodies diluted in Foxp3 permeabilization buffer for 40 min at 4 °C. Cell populations were acquired on BD LSR Fortessa, BD FACSCanto II or Cytoflex (Beckmann Coulter) flow cytometry devices or sorted using BD FACS Aria III. Data were processed using FlowJo software (v.10.6.0, BD Bioscience). An exemplified gating strategy is shown in Extended Data Fig. 9. The following antibodies were used: anti-CD4 (cl. GK1.5, 1:400 dilution), anti-CD8a (cl. 53-6.7, 1:400 dilution), anti-CD38 (cl. 90, 1:200 dilution), anti-CD44 (cl. IM7, 1:200 dilution), anti-CD62L (cl. MEL-14, 1:200 dilution), anti-CD45.1 (cl. A20, 1:200 dilution), anti-CD45.2 (cl. 104, 1:200 dilution), anti-CD45R (B220; cl. RA3-6B2, 1:200 dilution), anti-CD101 (cl. Moushi101, 1:200 dilution), anti-PD-1 (cl. J43, 1:200 dilution), anti-GL7 (cl. GL7, 1:200 dilution), anti-granzyme B (cl. NGZB, 1:150 dilution), anti-IFN-γ (cl. XMG1.2, 1:200 dilution), anti-ICOS (cl. C398.4A, 1:200 dilution),

anti-IL-2 (cl. JES6-5H4, 1:100 dilution), anti-KLRG1 (cl. 2F1, 1:100 dilution), anti-Ox40 (cl. OX-86, 1:200 dilution), anti-CTLA-4 (cl. UC10-4B9, 1:200 dilution), anti-Foxp3 (cl. FJK-16S, 1:100 dilution), anti-Ki67 (cl. SolA15, 1:200 dilution), anti-Tim3 (cl. RMT3-23, 1:200 dilution) and anti-TNF-α (cl. MP6-XT22, 1:100 dilution) all from eBioscience; anti-CD95 (cl. JO2, 1:200 dilution), anti-BATF (cl. S39-1060, 1:40 dilution) and anti-Bcl6 (K112-91, 1:50 dilution) all from BD Bioscience; anti-IL-17A (cl. TC11-18H10.1, 1:100 dilution), anti-CXCR5 (cl. L138D7, 1:50 dilution), anti-CD19 (cl. 6D5, 1:300 dilution), anti-IgD (cl. 11-26c.2a, 1:200 dilution), goat anti-rat antibody (cl. Poly4054, 1:200 dilution) all from BioLegend; and goat anti-rabbit antibody (Invitrogen, 1:200 dilution), anti-CD138 (cl. 281-2, BD Pharmingen, 1:200 dilution), anti-Roquin-1/2 (cl. 3F12, inhouse production, 1:10 dilution), anti-Regnase-1 (cl. 15D11, inhouse production, 1:10 dilution), anti-TCF-1 (cl. S33-966, BD Bioscience, 1:80 dilution), anti-TOX (cl. REA473, Miltenyi Biotech, 1:50 dilution) and anti-Rck (Bethyl).

AMNIS image stream measurements.

Cells were stained as described above and measured using the AMNIS image stream (Millipore).

Immunofluorescence microscopy.

Spleens were frozen in OCT compound (Tissue Tek), cryosections (7 μm) were prepared and fixed in acetone. Slides were stained with anti-IgD-PE (cl. 11-26c.2a, BioLegend) and anti-GL7-Alexa647 (cl. GL7, BioLegend). Images were acquired on an Olympus BX41 fluorescence microscope and processed with Fiji (v.1.0).

Seahorse measurements.

In vitro-deleted and activated $CD4^+$ and $CD8^+$ T cells were starved of IL-2 overnight and restimulated with anti-CD3e and anti-CD28 antibodies (0.5 μg ml^{-1}, BioLegend) for 6–7 h before the seahorse measurement. Cells were washed with PBS, resuspended in seahorse assay medium (XF RPMI, Agilent) containing 2 mM L-glutamine (Thermo Fisher Scientific), with or without 5 mM glucose (Sigma-Aldrich) for glycolytic or mitochondrial stress tests, respectively, and seeded on poly-L-lysine (50 μg ml^{-1}, Sigma-Aldrich) and goat anti-hamster (50 μg ml^{-1}) pre-coated plates at a density of 2–2.2 × 10^5 cells per well. Cells were degassed using a Cytation1 reader (BioTek) at 37 °C for 1 h. ECARs and OCRs were measured on a 96-well XFe Extracellular Flux Analyzer (Agilent). For each treatment three cycles of 3 min mixing and measurement each were performed. For normalization, nuclei stained with 8 μm Hoechst (Thermo Fisher Scientific) were counted in a Cytation1 reader. To assess basal glycolytic activity during the glycolytic stress test, the ECAR response to an acute 5-mM glucose (Sigma-Aldrich) injection was measured, followed by a 1.5μM oligomycin (Sigma-Aldrich) injection to inhibit mitochondrial respiration and induce maximal glycolytic capacity. Nonglycolytic acidification was assessed after injecting 50 mM 2-DG (Sigma-Aldrich). In the mitochondrial stress test 1.5 μM oligomycin was injected to inhibit mitochondrial proton flux. Maximal mitochondrial respiration was induced by injection of 1 μM FCCP (Sigma-Aldrich) and terminated by 0.5 μM rotenone (Sigma-Aldrich) and antimycin A (Sigma-Aldrich) injections.

Sucrose gradient fractionation.

Sucrose gradient fractionation was performed as described[48], with slight modifications. Shortly after, 5×10^7 $CD4^+$ T cells were washed in ice-cold PBS containing cycloheximide (0.1 mg ml^{-1}), resuspended in extraction buffer (20 mM Tris-HCl (pH 7.4), 140 mM KCl, 0.5 mM dithiothreitol (DTT), 5 mM $MgCl_2$, 0.5% Nonidet-P40, 0.1 mg ml^{-1} cycloheximide and protease inhibitor (PI)), incubated for 15 min on ice and centrifuged for 10 min at 12,000*g*. Extracts were layered onto a 4.7-ml sucrose gradient (18–50% sucrose (*w/v*) in 20 mM Tris-HCl, pH 7.4, 140 mM KCl, 0.5 mM DTT, 5 mM $MgCl_2$ and 0.1 mg ml^{-1} cycloheximide) and centrifuged at 4 °C in a SW55Ti rotor (Beckman) at 35,000 r.p.m. for 90 min. Gradients were fractionated into ten 0.5-ml fractions and absorbance profiles at 254 nm were recorded using the Piston gradient fractionator (Biocomp). For further protein analysis, polysome gradient fractions were subjected to TCA precipitation.

Culture of cell lines.

HeLa, HEK293T, P815 and B16-OVA cells were cultured in DMEM (Invitrogen) supplemented with 10% (*v/v*) FCS (Gibco), Pen-Strep (100 U ml^{-1}, each, Thermo Fisher Scientific), 10 mM HEPES, pH 7.2–7.5 (Invitrogen) at 37 °C and 10% CO_2. HEK293T, HeLa, B16-F10 (no. CRL-6475) and P815 (no. TIB-64) cell lines were purchased from ATCC. The B16-F10 cell line was retrovirally transduced with MigR1-OVA-GFP (provided by D. Zehn, TU Munich).

Calcium phosphate transfection for generation of retroviral particles.

HEK293T cells pre-treated with 25 μM chloroquine, were co-transfected with 5 μg of the packaging vector pCL-Eco (Addgene; 12371) and 50 μg of the respective pRetro-Xtight plasmids using calcium phosphate as a transfection reagent. After 6 h cells were washed and cultured in fresh medium for an additional 48 h. Viral particles were filtered (0.45 μM) and mixed with polybrene (10 μg ml^{-1}) before T cell transduction.

Expression plasmids.

For murine T cell reconstitution experiments, the GFP-coding sequence (CDS), the corresponding murine complete CDS or corresponding shortened versions, as indicated, of Roquin-1, Regnase-1, Regnase-2, Regnase-3 or Regnase-4 C-terminally fused to GFP were inserted into the pRetro-Xtight expression plasmid (Clontech) under the control of a Tet-responsive promotor. For FLIM/FRET experiments, murine Roquin-1 CDS fused C-terminally to the mCherry CDS or the Rck CDS C-terminally fused to eBFP2 was inserted into the pdest12.2 backbone (Invitrogen). For NanoBret assays, the complete CDS of Regnase-1 or Roquin-$1^{aa1\text{-}510}$ was inserted downstream of the HaloTag CDS in the pFN21A HaloTag CMV Vector (Promega) or NanoLuc CDS in the pFN31K Nluc CMV-neo Flexi Vector (Promega), respectively. Mutations in the CDS of Regnase-1 or Roquin-1 were inserted via the QuikChange site-directed-mutagenesis procedure (Stratagene). Primer sequences are available on request.

Cell lysis, SDS–PAGE and immunoblotting.

Cell lysis and SDS–PAGE were performed as described[42]. For immunoblotting, proteins were transferred to a PVDF membrane and analyzed using primary antibodies followed by horseradish peroxidase (HRP)-conjugated secondary antibodies (Cell Signaling). For protein detection, Amersham ECL Prime Western Blotting Detection Reagent and X-ray films were used. The following primary antibodies were used: Roquin-1/2 (cl. 3F12, monoclonal, inhouse production), Regnase-1 (cl. 15D11, inhouse production), Roquin-1 (A300-515A, polyclonal, Bethyl), GAPDH (cl. 6C5, Merck Millipore) and Rpl7a (Abcam, ab70753).

RNA isolation and RT–qPCR.

RNA isolation was performed by column-based RNA isolation utilizing the NucleoSpin RNA isolation kit (Macherey-Nagel) according to the manufacturer's protocol. RNA was transcribed into complementary DNA using the Quantitect RT kit (Roche) according to the manufacturer's protocol. To quantify gene expression, the UPL Probe Library System by Roche and the Roche Light Cycler 480 were utilized (Supplementary Table 2).

Co-immunoprecipitation.

To analyze interaction of Roquin and Regnase-1 proteins in T cells, co-immunoprecipitation was performed. T cells were lysed in lysis buffer (20 mM Tris-HCl (pH 7.5), 150 mM NaCl, 0.25% (*v/v*) Nonidet-P40, 1.5 mM $MgCl_2$, 1 mM DTT supplemented with 1× cOmplete, EDTA-free Protease Inhibitor Cocktail (Roche), 1× Halt Phosphatase Inhibitor Cocktail (Thermo Fisher) and 0.2 U μl^{-1} RNase inhibitor (RNasin, Promega)) on ice for 15 min and cleared by centrifugation for 15 min at 12.000*g* and 4 °C. Then, 10 µl Protein-A dynabeads (Invitrogen) were coupled under constant rotation to 10 µg Regnase-1 antibody (R&D systems, no. 604421) in lysis buffer at 4 °C overnight, followed by 1 h at 20 °C. After washing the antibody-coupled beads with phosphate-citrate buffer (24.4 mM citric acid, 65 mM sodium hydrogen phosphate (pH 5), supplemented with 1 mM DTT and PI), washed beads were incubated with 15 mg protein lysate in 900 µl lysis buffer for 4 h at 4 °C while continuously rotating. Then, beads were washed three times with lysis buffer (+ DTT and PI) and resuspended in 40 µl 1× Laemmli buffer. The samples were boiled at 95 °C for 5 min and co-immunoprecipitation was analyzed by SDS–PAGE and immunoblotting with monoclonal antibodies recognizing Regnase-1 (cl. 15D11) and Roquin (cl. 3F12).

NanoBret assay.

NanoBret assays were performed according to the protocol of the NanoBRET Nano-Glo Detection System (Promega). Between 4–6 h after seeding of 1×10^6 HEK293T cells into six-well plates, cells were transfected with 2 µg of HaloTag and 0.02 µg of NanoLuc expression plasmids using FuGENE reagent (Promega) according to the manufacturer's instructions. After 20 h, cells were trypsinized, resuspended in Opti-MEM I Reduced Serum Medium (no phenol red, with 4% FCS, Thermo Fisher Scientific), re-plated into 96-well plates and incubated with HaloTag NanoBRET 618 Ligand (100 nM final concentration) or dimethylsulfoxide as a no ligand negative control for 22 h. After addition of NanoBRET Nano-Glo Substrate the donor emission (460 nm) and acceptor emission (618 nm) was measured using the GloMax Discover System (Promega). The raw donor and acceptor

values were calculated and milliBRET units (mBU) were determined as mBU = acceptor emission (618 nm) / donor emission (460 nm) × 1,000 and afterwards corrected for background signal as mBRET = mean mBU experimental sample – mean mBU no ligand control.

FRET/FLIM experiments.

For confocal microscopy 1 d before analysis HeLa cells were transfected via calcium phosphate precipitation and cells were seeded 6 h before microscopic analysis on eight-well µ-Slides (glass bottom, Ibidi) in Leibovitz's L-15 medium (no phenol red, Thermo Fisher Scientific). For staining of the ER the cells were washed with HBSS (calcium, magnesium and no phenol red, Thermo Fisher Scientific) and incubated for 25 min at 37 °C in prewarmed staining solution (300 µl HBSS containing 0.8 µM ER-Tracker Red dye, Thermo Fisher Scientific). Confocal and FLIM images were performed with a TCS SP8X FALCON confocal head (Leica Microsystems) mounted on an inverted microscope (DMi8; Leica Microsystems). For confocal imaging, a 405-nm diode and a white-light laser were used as excitations sources (488 nm for GFP and 594 nm for mCherry). Single photons were collected through a 93×/1.3 NA glycerin-immersion objective and detected on Hybrid Detectors (HyD) (Leica Microsystems) with a 414–468 nm, 500–550 nm and 610–722 nm spectral detection window for BFP, GFP and mCherry detection, respectively. The image size was set to 512 × 512 pixels and a 2.5-fold zoom factor was applied, giving a pixel size of 0.098 µm and an image size of 50 × 50 µm. For FLIM, the white-light laser delivered 20 MHz repetition rate at 488 nm. Arrival time of single photons was measured with the included FALCON module and 60 frames were acquired at 1.17 Hz for each time-correlated single-photon counting recording, corresponding to a scanning speed of 600 Hz. FLIM image analyses were performed in the LAS X software. A threshold was applied to the lifetime images before analysis to eliminate background noise. Different regions of interest were fitted with a two-exponential decay model. The mean amplitude-weighted fluorescence lifetime of the area was extracted then reported. The FRET efficiency (E_{FRET}) was calculated according to the following formula:

$$E_{FRET} = 1 - (\tau_{DA} / \tau_{D})$$

where τ_{DA} is the lifetime of the donor–acceptor sample and τ_{D} is the lifetime of the donor alone. Lifetime images shown were produced using the phasor approach[49].

ELISA for detection of anti-nuclear antibodies.

Blood taken from hearts of male and female (age 6–12 weeks) mice was directly centrifuged at 10,000*g* for 10 min at 4 °C to collect serum. ANA ELISAs were performed using the mouse ANA total IgG ELISA kit (Alpha Diagnostic) according to the manufacturer's instructions. Optical density at 450 nm was measured on an ELISA reader (Versa Max Microplate reader, Molecular Devices) and concentrations were calculated by using standard serum as a reference.

Prediction of interacting residues on the Roquin surface.

The structures of the ROQ domain bound to RNA (PDB 4QI2) and ROQ-HEPN domain (PDB 4TXA) were superposed using PyMOL and a model of the ROQ-HEPN domain bound to the RNA stem loop was generated. Based on this model, residues on the Roquin surface that are typically involved in protein–protein interactions but not covered by RNA were mutated on the basis of stereochemical and/or electrostatic interference.

Expression and purification of GST–regnase-1^{D141N}.

Full-length GST–regnase-1^{D141N} was expressed from pGEX-6P-3 in *Escherichia coli* Rosetta 2 (DE3) pLysS. Cells were cultured at 37 °C in 2YT containing 50 μg ml^{-1} ampicillin, 35 μg ml^{-1} chloramphenicol and 30 μM $ZnCl_2$. At an optical density (OD_{600}) of 0.8, temperature was reduced to 18 °C and expression was induced by adding isopropyl β-D-1-thiogalactopyranoside (IPTG) to a concentration of 0.7 mM. After 16 h of incubation, cells were collected (5,200*g*, 4 °C, 30 min). Due to the fast degradation of the protein, the whole purification was conducted at 4 °C in one day. Cells were resuspended in lysis buffer (500 mM NaCl, 50 mM HEPES (pH 7.5), 2 mM $MgCl_2$, 30 μM $ZnCl_2$, 2 mM DTT, 1× cOmplete Protease Inhibitor Cocktail (Roche)) and sonicated on ice. After clarification of the lysate (30,000*g*, 4 °C, 30 min), supernatant was applied on a pre-equilibrated GSTrap column (GE Healthcare). After washing steps with high-salt buffer (1 M NaCl, 50 mM HEPES (pH 7.5), 2 mM $MgCl_2$, 30 μM $ZnCl_2$, 2 mM DTT) and re-equilibration in lysis buffer, bound proteins were eluted with lysis buffer containing 30 mM reduced glutathione. Eluted fractions were pooled and immediately loaded onto a heparin column (GE Healthcare) equilibrated in 100 mM NaCl, 20 mM HEPES (pH 7.5), 2 mM $MgCl_2$, 30 μM $ZnCl_2$ and 2 mM DTT and eluted using a linear gradient to 60% high-salt buffer in ten column volumes. Pooled fractions were further purified using a Superdex200 column (GE Healthcare) in gel filtration buffer (150 mM NaCl, 20 mM HEPES (pH 7.5), 2 mM $MgCl_2$, 30 μM $ZnCl_2$, 2 mM DTT). Protein-containing fractions were pooled and concentrated.

Expression and purification of GST–regnase-1$^{aa1\text{-}452;D141N}$.

His_6–GST–regnase-1$^{aa1\text{-}452:D141N}$ with an additional C-terminal His_6 tag was expressed from pOPINJ in *E. coli* Rosetta (DE3) cells. Cells were grown in LB medium with 34 μg ml^{-1} chloramphenicol and 100 μg ml^{-1} ampicillin at 37 °C. Expression of the protein was induced at OD_{600} 0.6 by adding 0.5 mM IPTG and overnight growing conditions changed to 18 °C. Next, cells were collected (6,238*g*, 15 min, 4 °C) and resuspended in lysis buffer (500 mM NaCl, 2 mM DTT, 2 mM $MgCl_2$, 30 μM $ZnCl_2$, PIs and 50 mM HEPES, pH 8) and sonicated on ice. The supernatant of the centrifugation (48,384*g*, 30 min, 4 °C) was applied to GSTrap column. The column was washed with high-salt buffer (1 M NaCl and 50 mM HEPES, pH 8) and the protein eluted using elution buffer (500 mM NaCl, 30 mM glutathione, 2 mM DTT, 2 mM $MgCl_2$, 30 μM $ZnCl_2$, PIs and 50 mM HEPES, pH 8). After changing the buffer to a low-salt buffer (50 mM NaCl, 35 μM $ZnCl_2$, 2 mM DTT, 2 mM $MgCl_2$ and HEPES, pH 8) the protein was loaded onto a heparin column. The bound protein was eluted with a gradient (20 column volumes 0–100%) using the same buffer including 1 M NaCl. Fractions were pooled, concentrated and further purified using a Superdex 75

10/300 GL column (Amersham Pharmacia Biosciences) in 150 mM NaCl, 35 μM $ZnCl_2$, 2 mM DTT and HEPES, pH 7.5 buffer.

Expression and purification of Roquin-1$^{aa2-440}$, SUMO–roquin-1$^{aa2-440}$ and its mutants.

His_6–SUMO–roquin-1$^{aa2-440}$ was expressed from pOPINS3C in *E. coli* BL21 Star (DE3). Roquin-1$^{aa2-440}$ and its mutants (Roquin-1$^{aa2-440;M199R}$, Roquin-1$^{aa2-440;L209Y}$, Roquin-1$^{aa2-440;E212K}$, Roquin-1$^{aa2-440;M199R/L209Y}$ and Roquin-1$^{aa2-440;M199R/E212K}$) were expressed as His_6-tagged proteins from pETM11 or pOPINF in *E. coli* BL21 (DE3) or BL21 Star (DE3). Cells were grown at 37 °C in LB medium with 50 μg ml^{-1} kanamycin (pETM11) or with 100 μg ml^{-1} ampicillin (pOPINS3C or pOPINF). At an OD_{600} of 0.4, cultures were induced by adding 0.5 mM IPTG and overnight growing conditions changed to 20 °C. Cells were collected (6,238*g*, 15 min, 4 °C), resuspended in lysis buffer (300 mM NaCl, 15 mM imidazole, 1 mg ml^{-1} lysozyme, 2 mM DTT, PIs and 50 mM Tris, pH 8) and sonicated on ice. After centrifugation (48,384*g*, 30 min, 4 °C), the supernatant was applied to a HisTrap column (GE Healthcare). Bound protein was eluted, concentrated and further purified using a Superdex 75 10/300 GL column (Amersham Pharmacia Biosciences) in 150 mM NaCl and 50 mM HEPES, pH 7.5 buffer.

Electrophoretic mobility shift assay.

The RNA fragment of Regnase-1 3′-UTR (nt194-212, IBA GmbH) was radioactively labeled using T4 polynucleotide kinase (Thermo Fisher Scientific) and [γ^{32}P] ATP (Hartmann Analytic) at 37 °C for 30 min. The reaction was stopped at 75 °C for 10 min. Sepharose spin columns (NucAway; Invitrogen) were used to separate RNA from free nucleotides. Radioactively labeled RNA (6 nM), proteins (GST–regnase-1$^{aa1-452;D141N}$, Roquin-1$^{aa2-440}$) and tRNA competitor (30 μg ml^{-1}) were incubated in HEPES/NaCl/$MgCl_2$ buffer (10 mM HEPES (pH 7.5), 150 mM NaCl and 2 mM $MgCl_2$) and 4% glycerol in a final volume of 20 μl for 30 min at 20 °C. Samples were resolved by native TBE–PAGE (4% polyacrylamide and 1× TBE buffer) or by gradient NativePAGE 4–16% Bis-Tris (Invitrogen) gels. Gels were analyzed using Fuji imaging plates exposed in the FLA-5100, after 10 min incubation in fixing solution (30% (*v/v*) methanol and 10% (*v/v*) acetic acid) and vacuum drying.

Competition pulldown assays of GST–regnase-1^{D141N} and Roquin variants.

Competition pulldowns were performed using GSTrap beads (GE Healthcare) pre-equilibrated in binding buffer (150 mM NaCl, 30 mM HEPES (pH 7.5), 2 mM $MgCl_2$, 30 μM $ZnCl_2$ and 2 mM DTT). Then, 0.5 nmol human full-length GST–regnase-1^{D141N} was mixed with 150 μl bead slurry and incubated for 10 min on ice. Subsequently, premixes of 1.2 nmol SUMO–roquin-1$^{aa2-440}$ wild-type and 1.2 nmol Roquin-1$^{aa2-440}$ mutant variants were added and incubated for 60 min at 4 °C. After four wash steps (950 μl binding buffer), bound proteins were eluted with 60 μl elution buffer (150 mM NaCl, 30 mM HEPES (pH 7.5), 2 mM $MgCl_2$, 30 μM $ZnCl_2$, 2 mM DTT and 30 mM reduced glutathione). Then, 5% input of individual proteins, wash fractions and elutions were analyzed on 12.5% SDS–PAGE, stained with Coomassie blue and imaged using a ChemiDoc XRS+ (BioRad). Band intensities of Roquin-1$^{aa2-440}$ mutant variants and SUMO–roquin-1$^{aa2-440}$ wild-type of three

independent experiments were quantified and averaged using Image Lab software and their ratio was plotted.

Surface plasmon resonance.

Binding between Roquin-1$^{aa2\text{-}440}$ and GST–regnase-1$^{aa1\text{-}452;D141N}$ was analyzed using BIACORE 3000 instrument (Biacore). Roquin-1$^{aa2\text{-}440}$ was coupled to the CM5 sensor chip (Biacore) at a concentration of 35 μg ml^{-1} in 10 mM sodium-phosphate buffer (pH 5.7). GST–regnase-1$^{aa1\text{-}452;D141N}$ was injected onto the sensor chip using the concentrations 0.032, 0.063, 0.125, 0.25, 0.5 and 1 μM at 30 μl min^{-1} flow rate in running buffer (150 mM NaCl, 35 μM $ZnCl_2$, 0.05% Tween20, 2 mM DTT and 10 mM HEPES, pH 7.5) at 20 °C. Acquired binding curves were double-referenced against the signal in the buffer run and a ligand-free reference channel. The equilibrium dissociation constant (K_D) was calculated from steady-state measurements using the BIAevaluation program (Biacore).

Statistical analysis and experimental design.

Statistical analysis was performed with Prism 5.0b (GraphPad) or Origin. *P* values were calculated with Student's *t*-test or one-way or two-way ANOVA, as indicated. Statistical significance was indicated. Error bars represent mean of all data points ± s.e.m. or mean ± s.d., as indicated. No statistical methods were used to predetermine sample sizes but our sample sizes are similar to those reported in previous publications[3,6,18,19]. Data distribution was assumed to be normal, but this was not formally tested. Experiments did not involve randomization of animals/samples or conditions or blinding of investigators. No animals or data points were excluded from analyses.

Extended Data

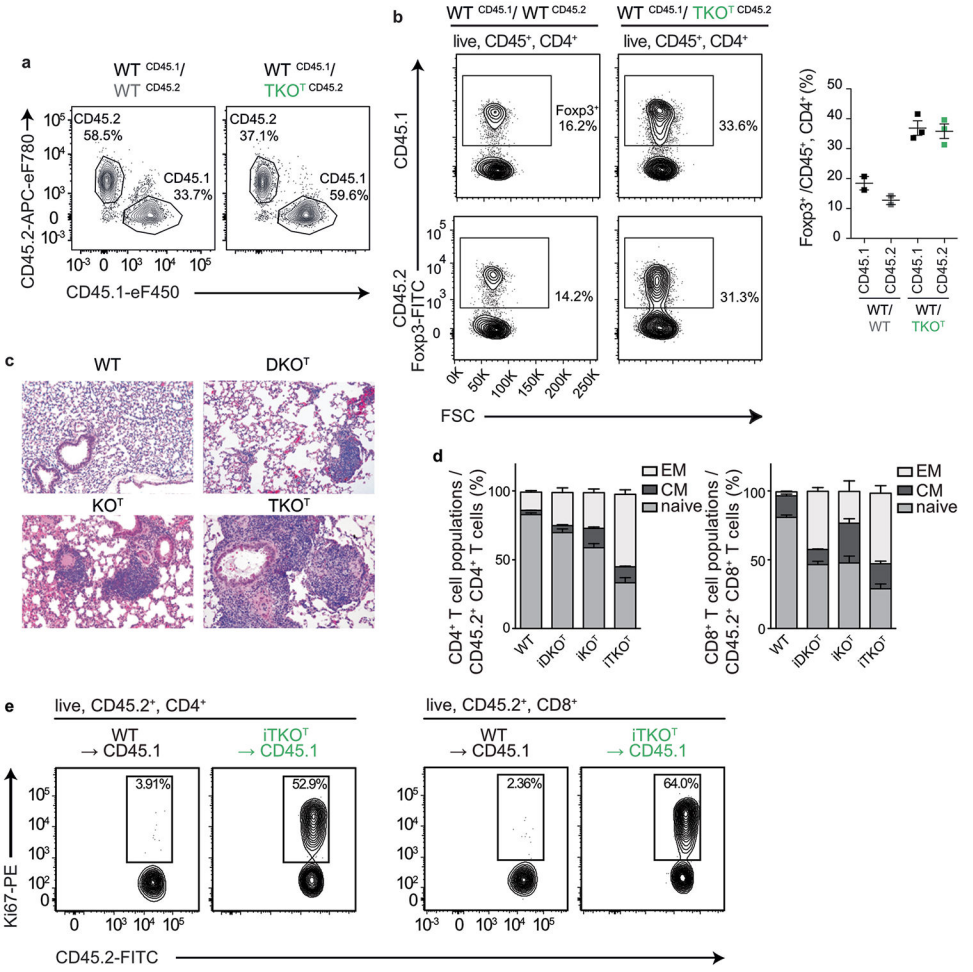

Extended Data Fig. 1 |. Roquin-1/2 and Regnase-1 maintain quiescence of T cells.

(**a**, **b**) Analysis of mixed bone marrow chimeric mice using either WT (CD45.2) and WT (CD45.1) or TKO^{T} (CD45.2) and WT (CD45.1) bone marrow cells injected into lethally irradiated CD45.1/2 recipient mice. Flow cytometry analysis of CD45.1 and CD45.2 cell populations (**a**) or T_{reg} cells (**b**) in splenocytes from recipient mice 9 weeks after reconstitution (WT CD45.1/WT CD45.2 recipients: n = 2, WT CD45.1/TKO CD45.2 recipients: n = 3, analyzed in one experiment). (**c**) H&E sections of lungs showing alveoli from WT, DKO^{T}, KO^{T} and TKO^{T} mice at the age of 6-8 weeks (Representative data of n ≥3 individual mice). (**d**, **e**) Analysis of CD45.2^{+} CD3^{+} T cells from Cre-ERt2 (WT), *Rc3h1/2*$^{fl/fl}$; Cre-ERt2 (iDKO), *Zc3h12a*$^{fl/fl}$; Cre-ERt2 (iKO) and *Rc3h1/2*$^{fl/fl}$; *Zc3h12a*$^{fl/fl}$; Cre-ERt2 (iTKO) mice that were adoptively transferred into WT CD45.1^{+} mice. Recipient mice were treated with tamoxifen by oral gavage to induce deletion of floxed alleles. On day 8 post transfer, T cells were analyzed for their ability to acquire an effector/memory phenotype (**d**) or to proliferate (**e**) within the host (n = 6 biological replicates).

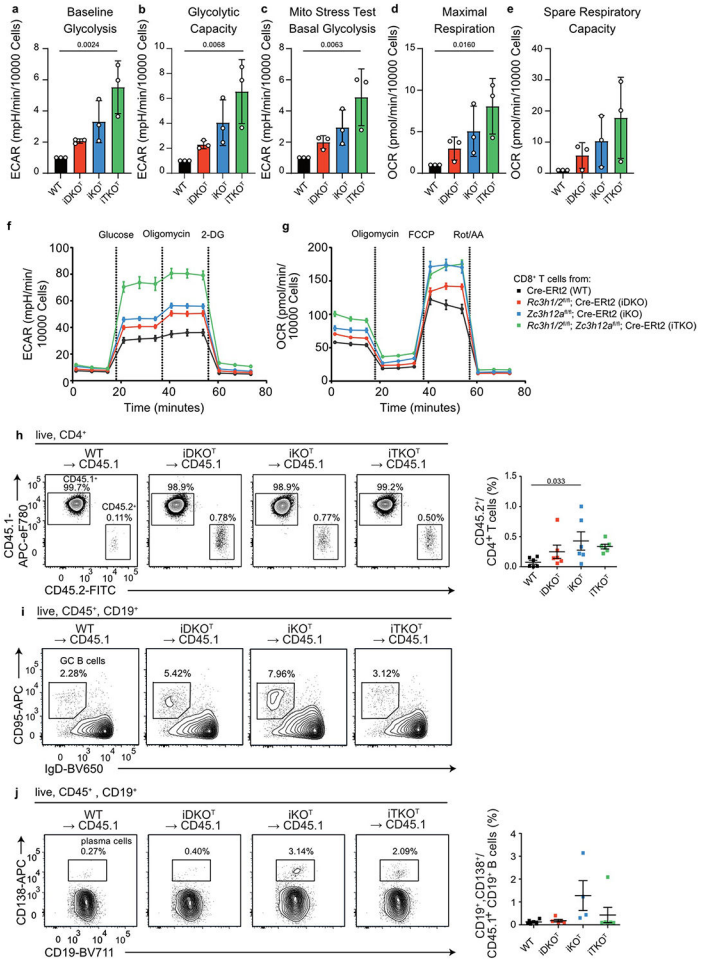

Extended Data Fig. 2 |. Roquin-1/2 and Regnase-1 control metabolism and humoral autoimmunity.

CD4$^+$ (**a–e**) or CD8$^+$ (**f**, **g**) T cells from Cre-ERt2 (WT), *Rc3h1/2*$^{fl/fl}$; Cre-ERt2 (iDKO), *Zc3h12a*$^{fl/fl}$; Cre-ERt2 (iKO) and *Rc3h1/2*$^{fl/fl}$; *Zc3h12a*$^{fl/fl}$; Cd4-Cre-ERt2 (iTKO) were treated with 4′-OH tamoxifen *in vitro* to induce deletion of floxed alleles. T cells were activated *in vitro* and expanded with IL-2 medium for 2d. IL-2 was withdrawn overnight before T cells were restimulated with anti-CD3/28 prior to glycolytic (**a**, **b**, **f**) and mitochondrial stress tests (**c–e**, **g**). Shown are calculated ratios for ECAR (mpH/min/10000 cells) (**a–c**) and OCR (pmol/min/10000 cells) (**d–e**) relative to WT, respectively. Naïve CD45.2$^+$ CD4$^+$ T cells from *Cd4*-Cre-ERt2 (WT), *Rc3h1/2*$^{fl/fl}$; *Cd4*-Cre-ERt2 (iDKO), *Zc3h12a*$^{fl/fl}$; *Cd4*-Cre-ERt2 (iKO) and *Rc3h1/2*$^{fl/fl}$; *Zc3h12a*$^{fl/fl}$; *Cd4*-Cre-ERt2 (iTKO) mice were adoptively transferred into CD45.1$^+$ recipient mice. Mice were treated with tamoxifen by oral gavage to induce deletion of floxed alleles. Adoptively transferred cells were identified by congenic markers on day 8 (**h**) or accumulation of germinal center B (**i**) or plasma cells (**j**) was determined on day 49 after induced deletion. (**a–e**) Data are presented as mean +/− SD of n = 3 biological replicates analyzed over 3 independent experiments, (**f**, **g**) representative of 3 independent experiments, (**h**) n = 6 analyzed mice, or (**i**, **j**) WT: n = 6, iDKO: n = 5, iKO: n = 4, iTKO: n = 6 in 2 independent experiments. Statistical significance was calculated by one-way ANOVA with Dunnett's post-hoc test.

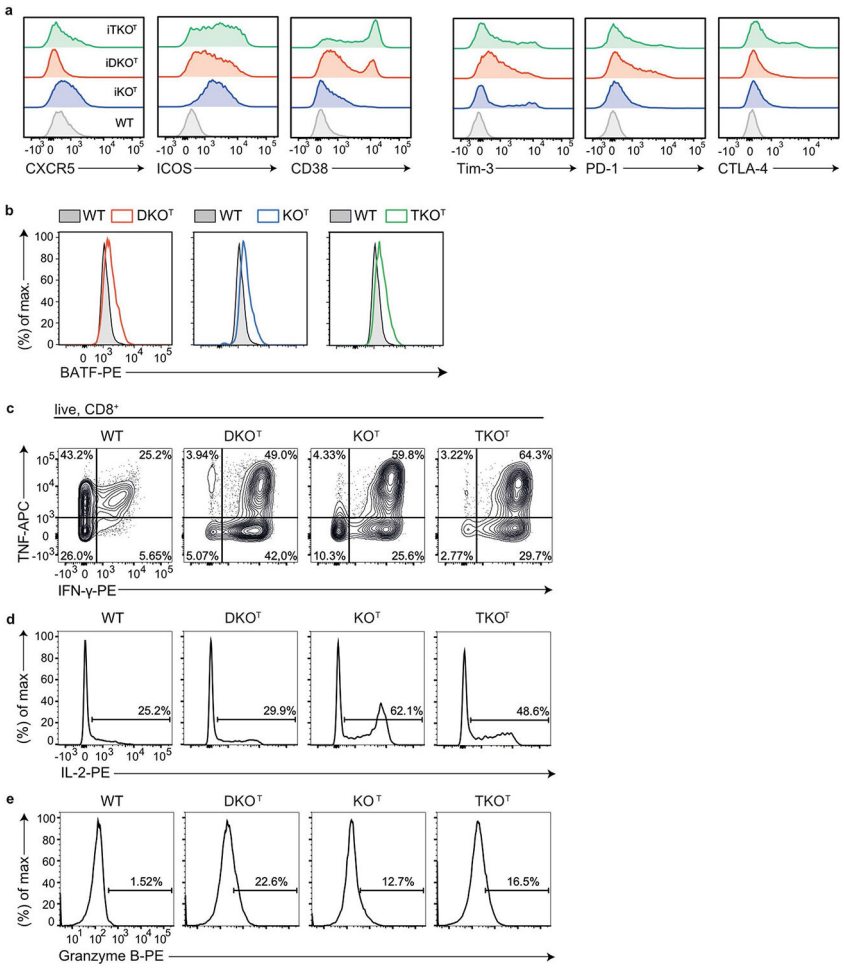

Extended Data Fig. 3 |. Describing phenotypes of DKO^T, KO^T and TKO^T CD8$^+$ T cells.

Flow cytometry analysis of markers of activation and exhaustion (**a**) and BATF transcription factor expression (**b**) in splenic WT, DKO^T, KO^T and TKO^T CD8$^+$ T cells. Data are representative of at least 5 individual 6-12 week old mice per genotype in at least two independent experiments. Flow cytometry analysis to Fig. 3e, f: intracellular cytokine staining of IFN-γ, TNF (**c**) and IL-2 (**d**) after PMA/ionomycin stimulation in CD8$^+$ T cells of splenocytes from WT, DKO^T, KO^T and TKO^T mice for 4 h. Histogram analysis to Fig. 3g: Granzyme B expression in splenic WT, DKO^T, KO^T and TKO^T CD8$^+$ T cells (**e**).

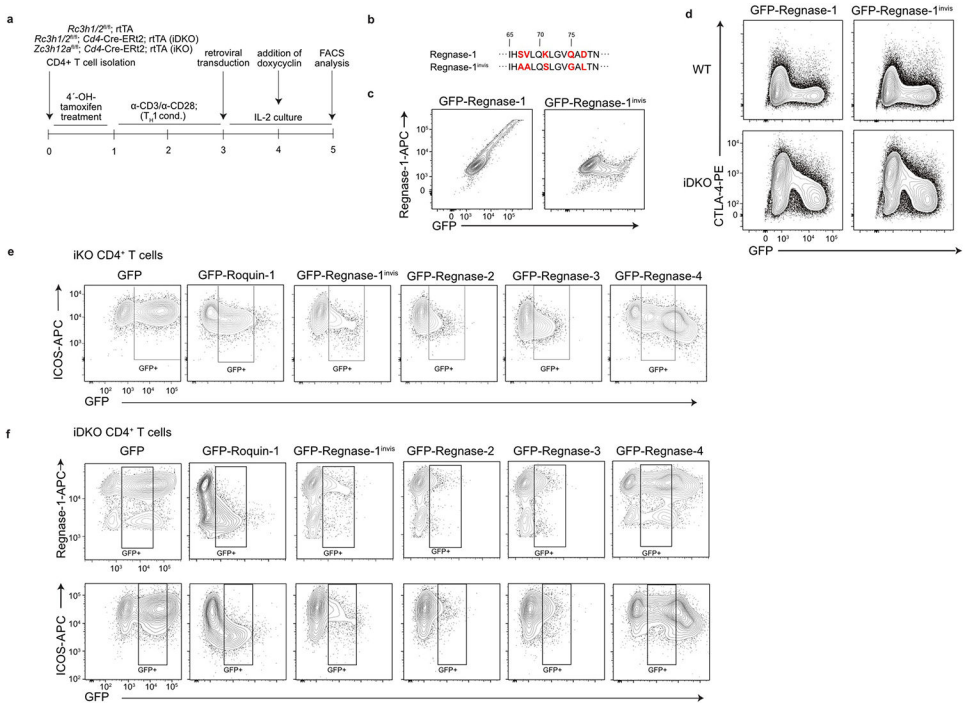

Extended Data Fig. 4 |. Regnase paralogs cannot complement for Roquin loss of function.
(**a**) Workflow of *in vitro* reconstitution experiments. (**b**) Mutations introduced in Regnase-1 coding sequence (marked in red) for the generation of an antibody-invisible GFP-tagged Regnase-1 construct (GFP-Regnase-1^{invis}). (**c**) Flow cytometry analysis of Regnase-1 expression after retroviral transduction of WT CD4$^+$ T cells with GFP-Regnase-1 or GFP-Regnase-1^{invis} constructs. (**d**) WT or iDKO CD4$^+$ T cells were retrovirally transduced with GFP–Regnase-1 or GFP-Regnase-1^{invis}. Contour plots of flow cytometry analysis of CTLA-4 expression in dependence of the GFP expression level. (**e**, **f**) Flow cytometry analysis of ICOS or Regnase-1 expression after retroviral transduction of iKO or iDKO CD4$^+$ T cells with the indicated GFP-fusion protein. Contour plots of histograms shown in Fig. 4c. (**d–f**) Data are representative of n = 3 independent experiments.

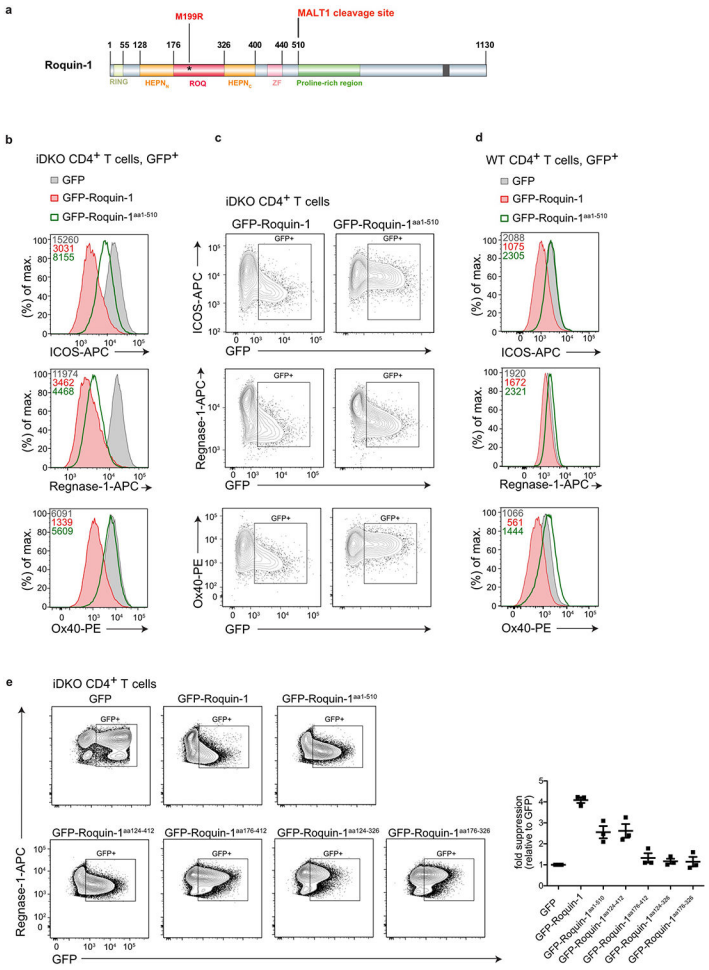

Extended Data Fig. 5 |. Dissecting protein domains of Roquin-1 sufficient for cooperative target regulation with Regnase-1.

(**a**) Schematic representation of Roquin-1 domain organization with indication of M199R mutation. iDKO (**b**, **c**) or WT (**d**) $CD4^+$ T cells were retrovirally transduced with GFP, GFP-Roquin-1 or GFP-Roquin-$1^{aa1\text{-}510}$ constructs. Histograms of flow cytometry analysis of ICOS, Regnase-1 or Ox40 expression, as indicated, in GFP^+ cells with indication of respective geometric MFI value. (**c**) Contour plots of histograms depicted in (**b**). (**e**) iDKO $CD4^+$ T cells were retrovirally transduced with the constructs encoding GFP, GFP-Roquin-1 or GFP-Roquin-1 mutant proteins. Flow cytometry analysis of Regnase-1 expression and quantification of fold suppression of Regnase-1 expression level in GFP^+ cells relative to cells expressing GFP control construct. (**b–e**) Data are representative of n = 3 independent experiments. (**e**) Data are presented as mean +/− SEM of n = 3 independent experiments.

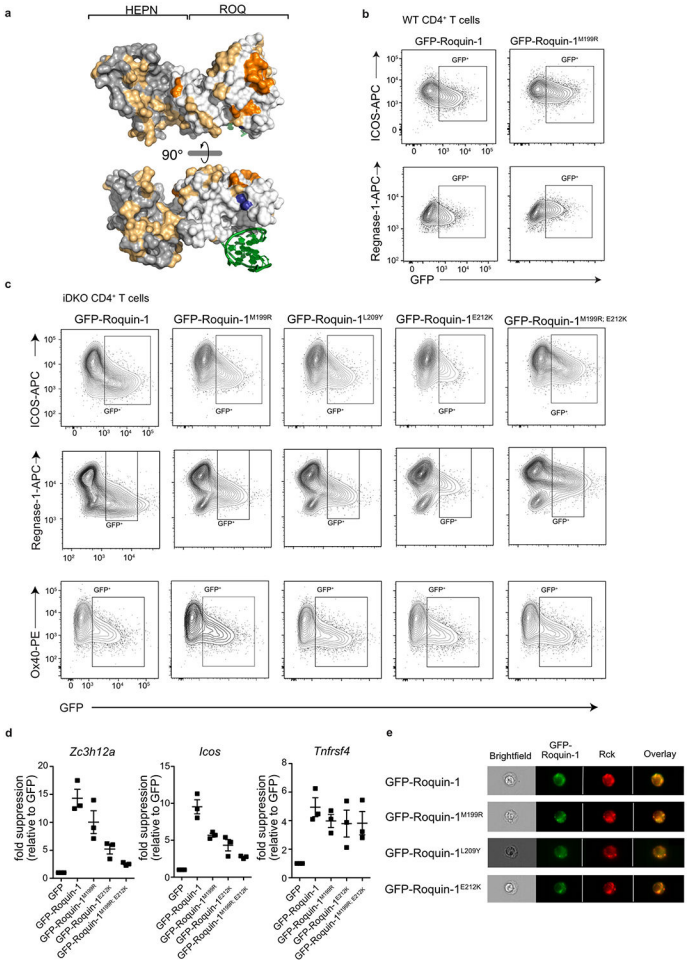

Extended Data Fig. 6 |. Functional validation of point mutations in Roquin-1 that reduce cooperation with Regnase-1.

(**a**) Structure of the Roquin-1 $HEPN_N$/ROQ/$HEPN_C$ domain with a bound RNA stem-loop marked in green. All amino acids tested are colored, essential amino acids for Roquin-1 and Regnase-1 interaction in the ROQ domain are marked in orange, non-essential ones in yellow and amino acid M199 in blue. WT (**b**) or iDKO (**c**) $CD4^+$ T cells were retrovirally transduced with GFP, GFP-Roquin-1 or the indicated GFP-Roquin-1 mutants. Contour plots of flow cytometry measurement of indicated targets in GFP^+ cells after 16 h of doxycycline induction of GFP-tagged constructs. (**b**) Contour plots of histograms shown in Fig. 4f or (**c**) shown in Fig. 4g. (**d**) iDKO $CD4^+$ T cells were retrovirally transduced with GFP, GFP-Roquin-1 or the indicated GFP-Roquin-1 mutants and sorted for GFP^+ cells 6 h after doxycycline induced expression of the respective constructs. The levels of *Zc3h12a*, Icos or *Tnfrsf4* mRNAs in GFP^+ cells were determined via RT-qPCR, normalized to *YWHAZ* and calculated as fold suppression of the respective construct relative to cells expressing the GFP control construct. Data show mean +/− SEM of n = 3 independent experiments. (**e**) Representative images of iDKO $CD4^+$ T cells transduced with the indicated GFP-Roquin-1 WT or mutant proteins, stained with anti-Rck (P-body marker) antibody and analyzed via Image Stream. (**b**, **c**) Data are representative of n = 3 independent experiments or (**e**) n = 2 independent experiments.

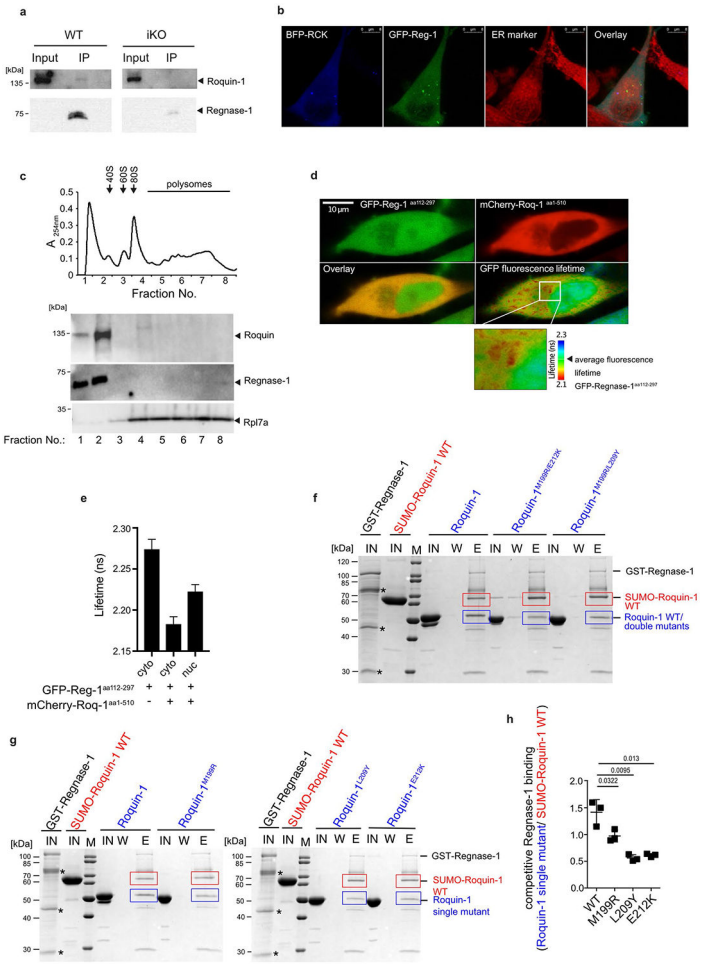

Extended Data Fig. 7 |. Molecular determinants of Roquin-1 interaction with Regnase-1. (**a**) Lysates of WT or iKO CD4$^+$ T cells were subjected to immunoprecipitation (IP) with antibodies against Regnase-1. Input lysates before IP and eluates from beads after IP were analyzed in immunoblots with antibodies against Roquin-1 or Regnase-1. (**b**, **d**) Fluorescence microscopy images of HeLa cells transfected with BFP-Rck and GFP-Regnase-1 (GFP-Reg-1) and stained with ER staining dye (**b**), or of cells transfected with GFP-Regnase-1$^{aa112\text{-}297}$ and mCherry-Roquin-1$^{aa1\text{-}510}$ (**d**). Quantification of GFP fluorescence lifetime in the cytoplasm (cyto) and nucleus (nuc) (**e**) of transfected cells shown in (**d**). (**c**) Cytoplasmic lysates of CD4$^+$ T cells were fractionated after sucrose gradient centrifugation and distribution of Roquin, Regnase-1 and Rpl7a proteins in the individual fractions analyzed via immunoblots, as indicated. Above, representative absorbance profile obtained during fractionation of gradients with indication of localization of 40 S and 60 S ribosomal subunits, 80 S monosomes and polysomes. (**f**, **g**) SDS-PAGE of competitive *in vitro* GST-pulldown experiments using GST-regnase-1^{D141N} and SUMO-roquin-1$^{aa2\text{-}440}$ in combination with the indicated untagged Roquin-1$^{aa2\text{-}440}$ double or single mutants. Purified proteins before pulldown (IN), supernatants of wash steps (W) as well as eluted proteins (E) were loaded. Asterisks mark the migration of degradation products of GST-regnase-1. (**h**) Quantification of eluted mutant Roquin-1$^{aa2\text{-}440}$ relative to SUMO-

roquin-1$^{aa2\text{-}440}$ wild-type protein of *in vitro* GST-pulldown experiments depicted in (**g**). (**b**, **d**, **f**, **g**) Depicted are representative data of n = 3 independent experiments or (**a**, **c**) of n = 2 independent experiments. (**e**) Data are presented as mean +/− SEM or (**h**) mean +/− SD and (**h**) statistical significance was calculated using t tests.

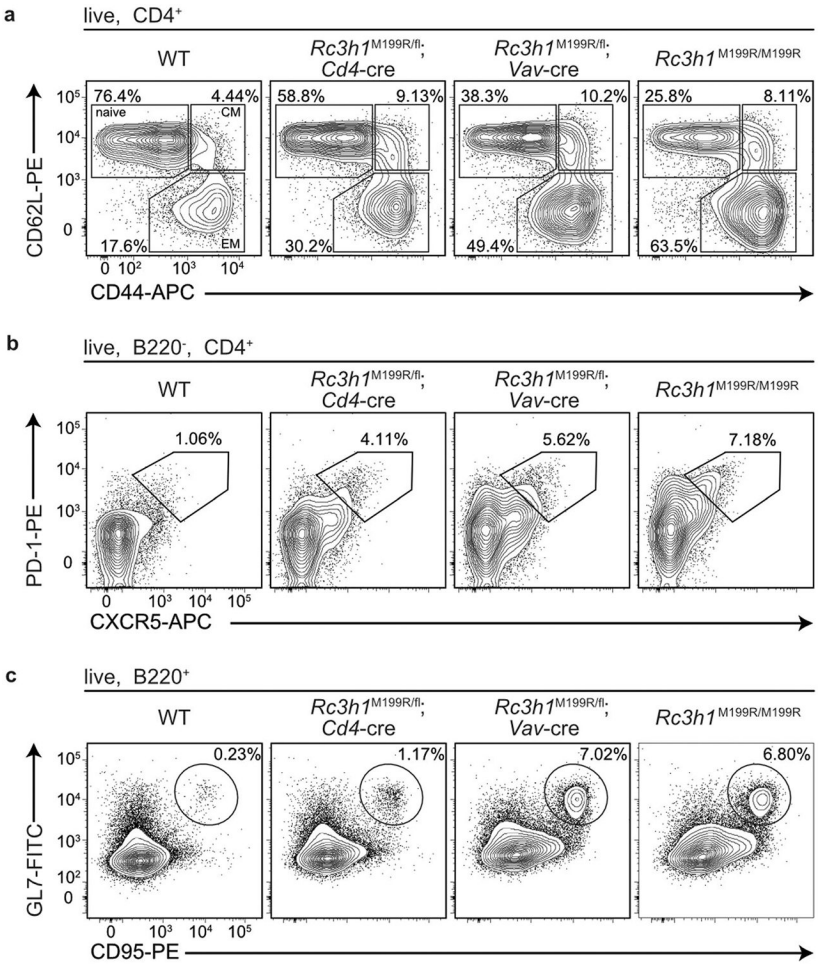

Extended Data Fig. 8 |. Phenotypes of mice with mutations impairing Roquin-1 interaction with Regnase-1.

Contour plots of flow cytometry analysis of CD4$^+$ T cells (**a**), T_{FH} cells (**b**) and GC B cells (**c**) from spleens of 9-14 weeks old WT, *Rc3h1*$^{M199R/fl}$;*Cd4*-Cre, *Rc3h1*$^{M199R/fl}$;*Vav*-Cre and *Rc3h1*$^{M199R/M199R}$ mice. Contour plots are representative of WT, *Rc3h1*$^{M199R/M199R}$: n = 6, *Rc3h1*$^{M199R/fl}$; *Cd4*-Cre, *Rc3h1*$^{M199R/fl}$; *Vav*-Cre: n = 5 (**a**), or WT, *Rc3h1*$^{M199R/M199R}$: n = 8, *Rc3h1*$^{M199R/fl}$; Cd4-Cre: n = 6, *Rc3h1*$^{M199R/fl}$; *Vav*-Cre: n = 7 (**b**, **c**) analyzed mice in at least 3 independent experiments.

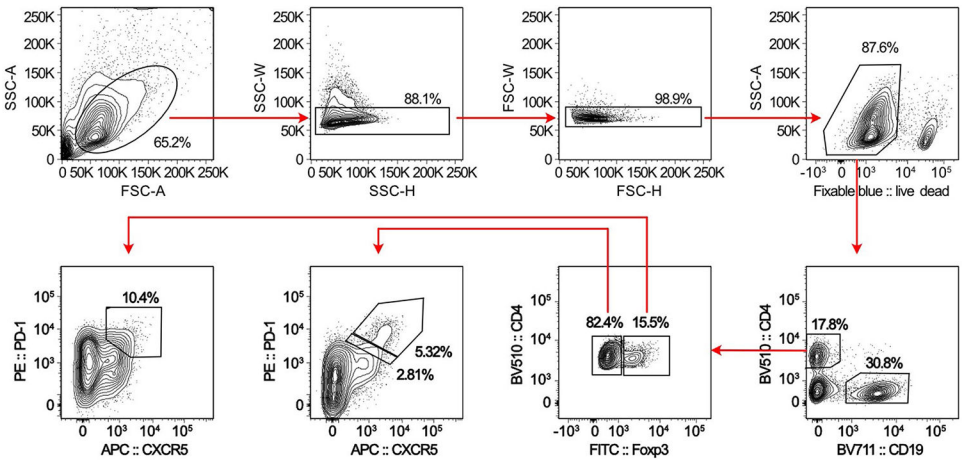

Extended Data Fig. 9 |. Exemplary gating strategy.

Cells were pregated on lymphocytes (FSC-A/SSC-A), single cells (SSC-H/SSC-W and FSC-H/FSC-W) and live cells (Fixable blue -) prior to gating on cell populations of interest.

Supplementary Material

Refer to Web version on PubMed Central for supplementary material.

Acknowledgements

We thank D.H. Busch (TU Munich) for critical reading of the manuscript. We thank C. Keplinger (Helmholtz Zentrum München) and L. Esser and J. Klein (Ludwig-Maximilians-Universität, Munich) for excellent technical support. We thank A. Blutke, J. Kranich and R. Schieweck (Ludwig-Maximilians-Universität, Munich) for support with histology and polysome profiles and the BMC Core Facility (Ludwig-Maximilians-Universität, Munich) for support in flow cytometry and the immunoanalytics platform for their support in chromium release assays (E. Noessner, Helmholtz Zentrum München). For the provision of NanoBret constructs we thank K.-P. Knobeloch (University Clinic Freiburg) and D. Zehn (TU Munich) for providing the MigR1-OVA-GFP retroviral plasmid. The work was supported by the German Research Foundation grants SPP-1935 (to D.N. and V.H.), SFB-TRR338 (projects C02 to V.H. and C05 to S.T.), SFB-1054 (project A03) as well as HE3359/7-1 and HE3359/8-1 to V.H. and under Germany's Excellence Strategy within the framework of the Munich Cluster for Systems Neurology (EXC 2145 SyNergy, ID 390857198 to W.W.) and SFB-870 (project A13 to W.W.) as well as grants from the Wilhelm Sander, Fritz Thyssen, Else Kröner-Fresenius and Krebshilfe foundations to V.H.

Data availability

All data are provided in the article and its supplementary files or from the corresponding author upon reasonable request. For analysis of the Roquin structure the publicly available structural datasets of Roquin-1 ROQ domain bound to RNA (PDB 4QI2) and Roquin-1 ROQ-HEPN domain (PDB 4TXA) were used. Source data are provided with this paper.

References

1. Pratama A et al. Roquin-2 shares functions with its paralog Roquin-1 in the repression of mRNAs controlling T follicular helper cells and systemic inflammation. Immunity 38, 669–680 (2013). [PubMed: 23583642]
2. Tavernier SJ et al. A human immune dysregulation syndrome characterized by severe hyperinflammation with a homozygous nonsense Roquin-1 mutation. Nat. Commun 10, 4779 (2019). [PubMed: 31636267]

3. Vogel KU et al. Roquin paralogs 1 and 2 redundantly repress the Icos and Ox40 costimulator mRNAs and control follicular helper T cell differentiation. Immunity 38, 655–668 (2013). [PubMed: 23583643]
4. Matsushita K et al. Zc3h12a is an RNase essential for controlling immune responses by regulating mRNA decay. Nature 458, 1185–1190 (2009). [PubMed: 19322177]
5. Uehata T et al. Malt1-induced cleavage of regnase-1 in $CD4^+$ helper T cells regulates immune activation. Cell 153, 1036–1049 (2013). [PubMed: 23706741]
6. Jeltsch KM et al. Cleavage of roquin and regnase-1 by the paracaspase MALT1 releases their cooperatively repressed targets to promote $T_{(H)}17$ differentiation. Nat. Immunol 15, 1079–1089 (2014). [PubMed: 25282160]
7. Mino T et al. Regnase-1 and Roquin regulate a common element in inflammatory mRNAs by spatiotemporally distinct mechanisms. Cell 161, 1058–1073 (2015). [PubMed: 26000482]
8. Jeltsch KM & Heissmeyer V Regulation of T cell signaling and autoimmunity by RNA-binding proteins. Curr. Opin. Immunol 39, 127–135 (2016). [PubMed: 26871597]
9. Leppek K et al. Roquin promotes constitutive mRNA decay via a conserved class of stem-loop recognition motifs. Cell 153, 869–881 (2013). [PubMed: 23663784]
10. Glasmacher E et al. Roquin binds inducible costimulator mRNA and effectors of mRNA decay to induce microRNA-independent post-transcriptional repression. Nat. Immunol 11, 725–733 (2010). [PubMed: 20639877]
11. Sgromo A et al. A CAF40-binding motif facilitates recruitment of the CCR4-NOT complex to mRNAs targeted by *Drosophila* Roquin. Nat. Commun 8, 14307 (2017). [PubMed: 28165457]
12. Mino T et al. Translation-dependent unwinding of stem-loops by UPF1 licenses Regnase-1 to degrade inflammatory mRNAs. Nucleic Acids Res. 47, 8838–8859 (2019). [PubMed: 31329944]
13. Fu M & Blackshear PJ RNA-binding proteins in immune regulation: a focus on CCCH zinc finger proteins. Nat. Rev. Immunol 17, 130–143 (2017). [PubMed: 27990022]
14. Vinuesa CG et al. A RING-type ubiquitin ligase family member required to repress follicular helper T cells and autoimmunity. Nature 435, 452–458 (2005). [PubMed: 15917799]
15. Akira S Regnase-1, a ribonuclease involved in the regulation of immune responses. Cold Spring Harb. Symp. Quant. Biol 78, 51–60 (2013). [PubMed: 24163394]
16. Heissmeyer V & Vogel KU Molecular control of T_{FH} cell differentiation by Roquin family proteins. Immunol. Rev 253, 273–289 (2013). [PubMed: 23550652]
17. von Gamm M et al. Immune homeostasis and regulation of the interferon pathway require myeloid-derived Regnase-3. J. Exp. Med 216, 1700–1723 (2019). [PubMed: 31126966]
18. Wei J et al. Targeting Regnase-1 programs long-lived effector T cells for cancer therapy. Nature 576, 471–476 (2019). [PubMed: 31827283]
19. Zheng W et al. Regnase-1 suppresses $TCF\text{-}1^+$ precursor exhausted T cell formation to limit CAR-T-cell responses against ALL. Blood 138, 122–135 (2021). [PubMed: 33690816]
20. Li Y et al. Central role of myeloid MCPIP1 in protecting against LPS-induced inflammation and lung injury. Signal Transduct. Target Ther 2, 17066 (2017). [PubMed: 29263935]
21. Bertossi A et al. Loss of Roquin induces early death and immune deregulation but not autoimmunity. J. Exp. Med 208, 1749–1756 (2011). [PubMed: 21844204]
22. Cui X et al. Regnase-1 and Roquin nonredundantly regulate T_H1 differentiation causing cardiac inflammation and fibrosis. J. Immunol 199, 4066–4077 (2017). [PubMed: 29127149]
23. Ventura A et al. Restoration of p53 function leads to tumour regression in vivo. Nature 445, 661–665 (2007). [PubMed: 17251932]
24. Sledzinska A TGF-β signalling is required for $CD4^+$ T cell homeostasis but dispensable for regulatory T cell function. PLoS Biol. 11, e1001674 (2013). [PubMed: 24115907]
25. Zeitrag J, Alterauge D, Dahlstrom F & Baumjohann D Gene dose matters: considerations for the use of inducible CD4-CreER(T2) mouse lines. Eur. J. Immunol 50, 603–605 (2020). [PubMed: 32087088]
26. Hudson WH et al. Proliferating transitory T cells with an effector-like transcriptional signature emerge from $PD\text{-}1^+$ stem-like $CD8^+$ T cells during chronic infection. Immunity 51, 1043–1058 (2019). [PubMed: 31810882]

27. McLane LM, Abdel-Hakeem MS & Wherry EJ CD8 T cell exhaustion during chronic viral infection and cancer. Annu Rev. Immunol 37, 457–495 (2019). [PubMed: 30676822]
28. Yu D et al. Roquin represses autoimmunity by limiting inducible T-cell co-stimulator messenger RNA. Nature 450, 299–303 (2007). [PubMed: 18172933]
29. Tan AH, Wong SC & Lam KP Regulation of mouse inducible costimulator (ICOS) expression by Fyn-NFATc2 and ERK signaling in T cells. J. Biol. Chem 281, 28666–28678 (2006). [PubMed: 16880206]
30. Iwasaki H et al. The IκB kinase complex regulates the stability of cytokine-encoding mRNA induced by TLR-IL-1R by controlling degradation of regnase-1. Nat. Immunol 12, 1167–1175 (2011). [PubMed: 22037600]
31. Janowski R et al. Roquin recognizes a non-canonical hexaloop structure in the 3′-UTR of Ox40. Nat. Commun 7, 11032 (2016). [PubMed: 27010430]
32. Schlundt A et al. Structural basis for RNA recognition in roquin-mediated post-transcriptional gene regulation. Nat. Struct. Mol. Biol 21, 671–678 (2014). [PubMed: 25026077]
33. Srivastava M et al. Roquin binds microRNA-146a and Argonaute2 to regulate microRNA homeostasis. Nat. Commun 6, 6253 (2015). [PubMed: 25697406]
34. Tan D, Zhou M, Kiledjian M & Tong L The ROQ domain of Roquin recognizes mRNA constitutive-decay element and double-stranded RNA. Nat. Struct. Mol. Biol 21, 679–685 (2014). [PubMed: 25026078]
35. Suzuki HI et al. MCPIP1 ribonuclease antagonizes dicer and terminates microRNA biogenesis through precursor microRNA degradation. Mol. Cell 44, 424–436 (2011). [PubMed: 22055188]
36. Lee SK et al. Interferon-γ excess leads to pathogenic accumulation of follicular helper T cells and germinal centers. Immunity 37, 880–892 (2012). [PubMed: 23159227]
37. Ellyard JI et al. Heterozygosity for Roquinsan leads to angioimmunoblastic T-cell lymphoma-like tumors in mice. Blood 120, 812–821 (2012). [PubMed: 22700722]
38. Blank CU et al. Defining 'T cell exhaustion'. Nat. Rev. Immunol 19, 665–674 (2019). [PubMed: 31570879]
39. Essig K et al. Roquin targets mRNAs in a 3′-UTR-specific manner by different modes of regulation. Nat. Commun 9, 3810 (2018). [PubMed: 30232334]
40. Murakawa Y et al. RC3H1 post-transcriptionally regulates A20 mRNA and modulates the activity of the IKK/NF-κB pathway. Nat. Commun 6, 7367 (2015). [PubMed: 26170170]
41. Song J et al. Human cytomegalovirus induces and exploits Roquin to counteract the IRF1-mediated antiviral state. Proc. Natl Acad. Sci. USA 116, 18619–18628 (2019). [PubMed: 31451648]
42. Essig K et al. Roquin suppresses the PI3K-mTOR signaling pathway to inhibit T helper cell differentiation and conversion of T_{reg} to Tfr cells. Immunity 47, 1067–1082 e12 (2017). [PubMed: 29246441]
43. Nagahama Y et al. Regnase-1 controls colon epithelial regeneration via regulation of mTOR and purine metabolism. Proc. Natl Acad. Sci. USA 115, 11036–11041 (2018). [PubMed: 30297433]
44. Hoefig KP et al. Defining the RBPome of primary T helper cells to elucidate higher-order Roquin-mediated mRNA regulation. Nat. Commun 12, 5208 (2021). [PubMed: 34471108]

References

45. Lee PP et al. A critical role for Dnmt1 and DNA methylation in T cell development, function, and survival. Immunity 15, 763–774 (2001). [PubMed: 11728338]
46. Hogquist KA et al. T cell receptor antagonist peptides induce positive selection. Cell 76, 17–27 (1994). [PubMed: 8287475]
47. Hochedlinger K, Yamada Y, Beard C & Jaenisch R Ectopic expression of Oct-4 blocks progenitor-cell differentiation and causes dysplasia in epithelial tissues. Cell 121, 465–477 (2005). [PubMed: 15882627]
48. Schieweck R et al. Pumilio2 and Staufen2 selectively balance the synaptic proteome. Cell Rep. 35, 109279 (2021). [PubMed: 34161769]

49. Digman MA, Caiolfa VR, Zamai M & Gratton E The phasor approach to fluorescence lifetime imaging analysis. Biophys. J 94, L14–L16 (2008). [PubMed: 17981902]

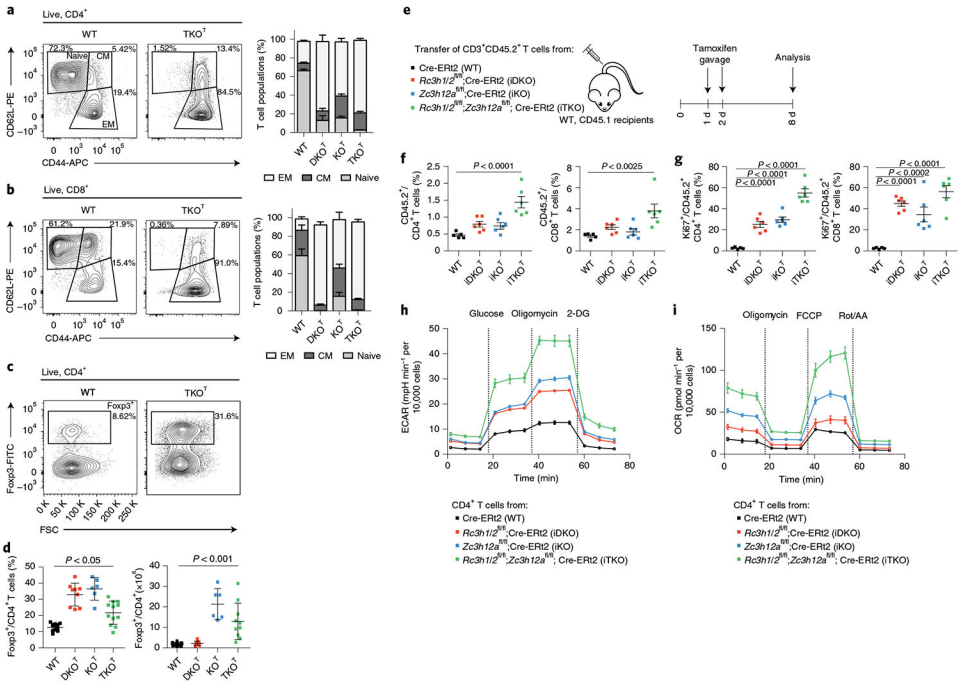

Fig. 1 | Roquin-1/2 and Regnase-1 maintain quiescence of T cells.

a–d, Flow cytometry analysis of $CD4^+$ (**a**), $CD8^+$ (**b**) subpopulations (WT, $n = 9$; DKO^T and KO^T, $n = 6$; TKO^T, $n = 5$ mice analyzed in at least three independent experiments) and T_{reg} cells (**c**,**d**) (WT, $n = 15$; DKO^T, $n = 9$; KO^T, $n = 6$; TKO^T, $n = 10$ mice analyzed in at least three independent experiments) from spleens of 6–8-week-old WT, DKO^T, KO^T and TKO^T mice. CM, central memory; EM, effector memory; WT, wild type. **e**, $CD45.2^+CD3^+$ T cells from WT, iDKO, iKO and iTKO mice were adoptively transferred into WT $CD45.1^+$ mice. Mice were treated with tamoxifen by oral gavage to induce deletion of floxed alleles. **f**,**g**, Frequency (**f**) and proliferation (**g**) of $CD45.2^+$, $CD4^+$ and $CD45.2^+$, $CD8^+$ T cells were analyzed by flow cytometry on day 8 after transfer ($n = 6$ biological replicates). **h**,**i**, $CD4^+$ T cells from WT, iDKO, iKO and iTKO mice were treated with 4′-OH-tamoxifen in vitro to induce deletion of floxed alleles. T cells were kept under type 1 helper T cell conditions and expanded with IL-2-containing medium for 2 d. IL-2 was withdrawn overnight followed by restimulation with anti-CD3/28 before glycolytic (**h**) and mitochondrial stress testing (**i**) ($n = 3$ independent experiments). 2-DG, 2-deoxyglucose; Rot, rotenone; AA, antimycin. Data are presented as mean ± s.e.m., analyzed by one-way analysis of variance (ANOVA) with Bonferroni (**d**) or Dunnett's (**f**,**g**) post hoc test.

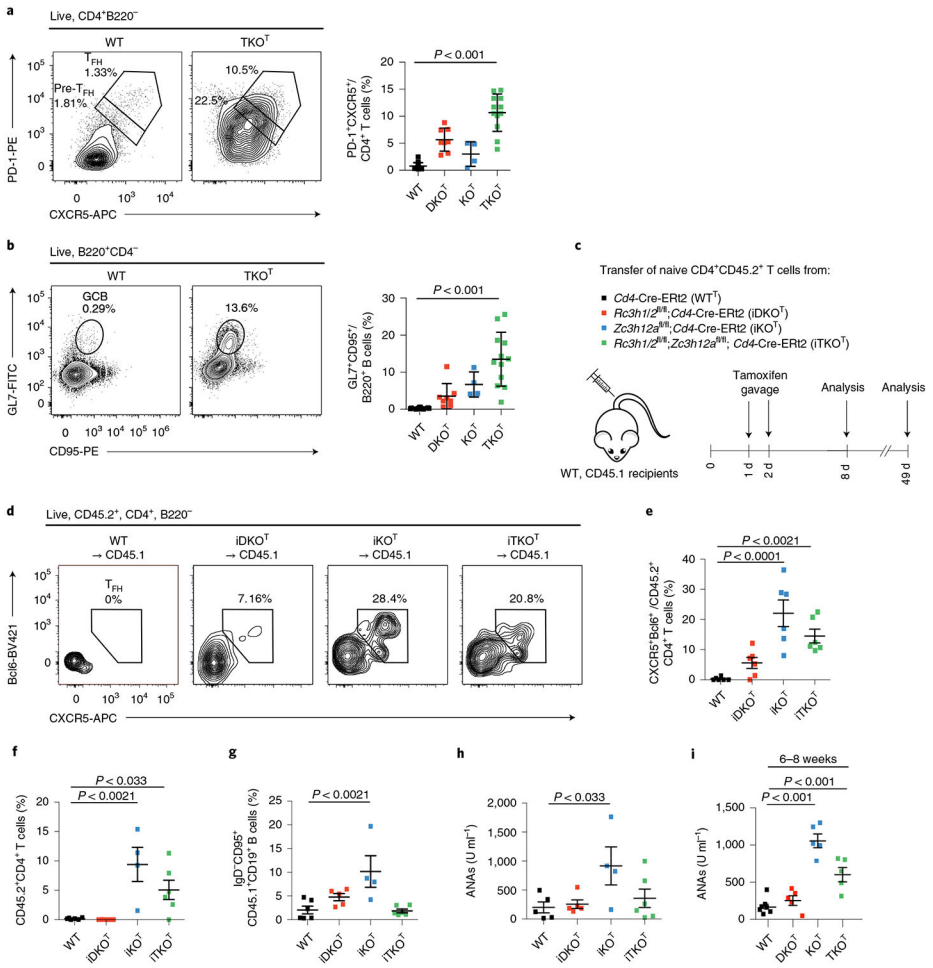

Fig. 2 | Roquin-1/2 and Regnase-1 control T_{FH} differentiation and humoral autoimmunity. **a**,**b**, Flow cytometry analysis of T_{FH} (**a**) and GC B cell (**b**) subpopulations from spleens of 6–8-week-old WT, DKO^T, KO^T and TKO^T mice (WT, $n = 14$; DKO^T, $n = 8$; KO^T, $n = 4$; TKO^T, $n = 12$ analyzed mice in at least three independent experiments). **c**, Naive $CD45.2^+CD4^+$ T cells from WT, iDKO, iKO and iTKO mice were adoptively transferred into congenic WT CD45.1 mice. Mice were treated with tamoxifen by oral gavage to induce deletion of floxed alleles. **d**,**e**, Adoptively transferred T cells were analyzed by flow cytometry for markers of T_{FH} cell differentiation on day 8 after transfer ($n = 6$ biological replicates). **f–h**, Frequencies of adoptively transferred WT, iDKO, iKO and iTKO $CD45.2^+CD4^+$ T cells (**f**), frequencies of recipient GC B cells (**g**) as well as levels of ANAs in the sera of recipient mice (**h**) were determined on day 49 after transfer (WT, $n = 6$; iDKO, $n = 5$; iKO, $n = 4$; iTKO, $n = 6$). **i**, ANAs in the serum of 6–8-week-old WT, DKO^T, KO^T and TKO^T mice (WT, $n = 7$; DKO^T, KO^T and TKO^T, $n = 5$ analyzed mice in three independent experiments). All data are presented as mean ± s.e.m. Statistical significance was calculated by one-way ANOVA with Bonferroni post hoc test (**a**,**b**) or Dunnett's post hoc test (**e–i**).

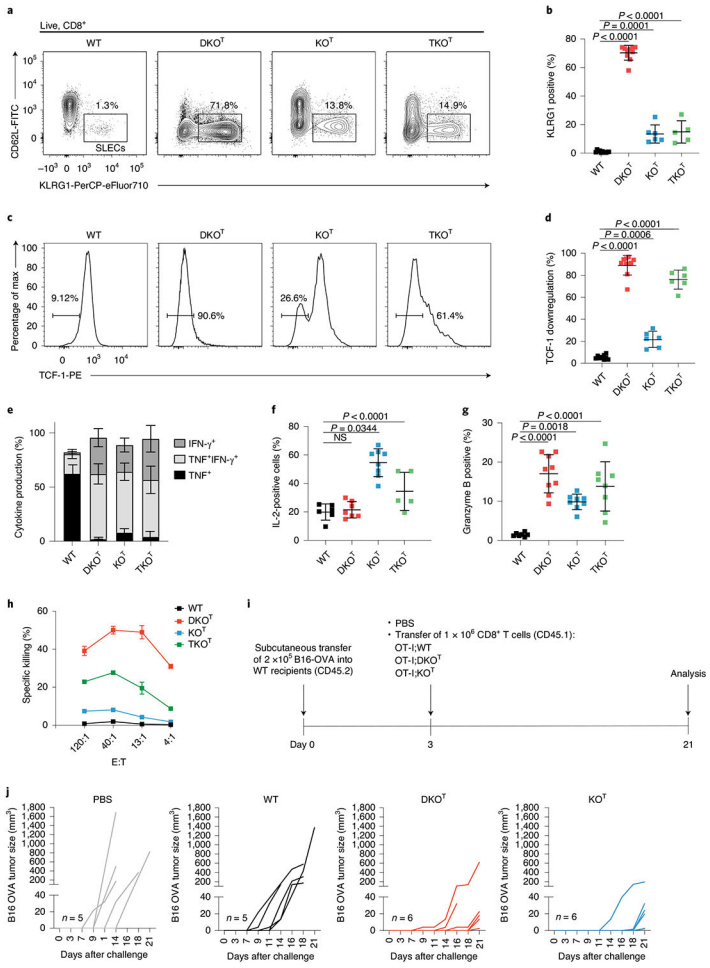

Fig. 3 | Inactivation of Roquin-1/2 or Regnase-1 in CD8$^+$ T cells enhances cytotoxicity.

a–d, Flow cytometry analysis of splenic WT, DKO^T, KO^T and TKO^T CD8$^+$ T cells for KLRG1 and CD62L expression (**a**), frequencies of SLEC CD8$^+$ T cells (WT, n = 11; iDKO, n = 10; iKO, n = 6; iTKO, n = 5 individual mice in three independent experiments) (**b**) and percentage of cells with TCF-1 downregulation (WT, n = 9; iDKO, n = 10; iKO, n = 6; iTKO, n = 6 individual mice in three independent experiments) (**c**,**d**). **e**,**f**, Quantification of intracellular cytokine staining of IFN-γ, TNF (WT, n = 9; iDKO, n = 9; iKO, n = 11; iTKO, n = 5 individual mice in three independent experiments) (**e**) and IL-2 (WT, n = 6; iDKO, n = 7; iKO, n = 8; iTKO, n = 5 individual mice in three independent experiments) (**f**) in CD8$^+$ T cells after PMA/ionomycin stimulation for 4 h. NS, not significant. **g**, Quantification of granzyme B-positive CD8$^+$ T cells (WT, n = 7; iDKO, n = 11; iKO, n = 8; iTKO, n = 9 individual mice in four independent experiments) in spleens from WT, DKO^T, KO^T and TKO^T mice. **h**, Chromium-release assay of P815 cells cultivated in effector to target ratios as indicated 4 h after adding splenic CD8$^+$ T cells isolated from WT, DKO^T, KO^T and TKO^T mice (n = 2 individual mice in one experiment). **i**, Schematic representation of the experimental set-up of the B16-OVA tumor model. **j**, B16-OVA tumor growth without transfer (PBS control n = 5) or after transfer of either WT (n = 5), DKO^T or KO^T OT-I

T cells (n = 6 individual mice in one experiment). Data are presented as mean ± s.e.m. Statistical significance was calculated by one-way ANOVA with Dunnett's post hoc test.

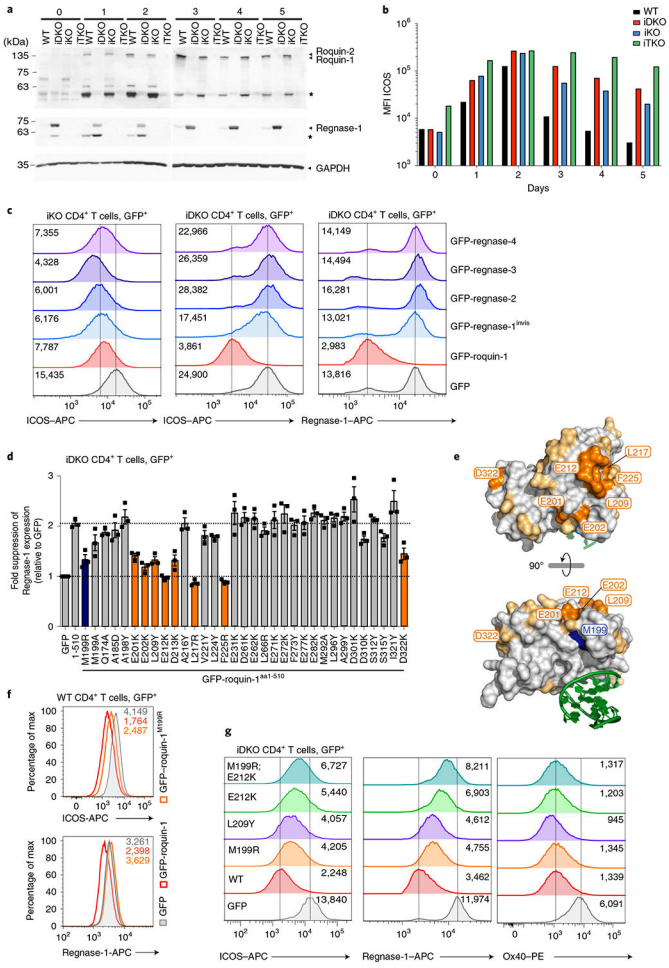

Fig. 4 | Functional definition of Roquin-1 interaction with Regnase-1.

a,**b**, WT, iDKO, iKO and iTKO CD4$^+$ T cells were deleted in vivo by tamoxifen gavage, activated in vitro with anti-CD3/28 under T_H1 cell conditions (days 0–2) and cultivated in medium containing IL-2 (days 3–5). For each day, expression of Roquin-1/Roquin-2, Regnase-1 and GAPDH (**a**) or ICOS (**b**) was analyzed by immunoblot or flow cytometry, respectively. Asterisks mark MALT1 cleavage fragments of Roquin-1 and Regnase-1 (**a**). MFI, mean fluorescence intensity. **c**,**d** CD4$^+$ T cells of indicated genotypes were retrovirally transduced with GFP, GFP–roquin-1, GFP–regnase-1^{invis}, GFP–regnase-2, GFP–regnase-3, GFP–regnase-4 (**c**) or with GFP, GFP–roquin-1$^{aa1\text{-}510}$ and ROQ mutants introduced into GFP–roquin-1$^{aa1\text{-}510}$ (**d**). Histograms of ICOS and Regnase-1 expression in GFP$^+$ cells with indication of the respective geometric MFI (gMFI) values (**c**) or fold suppression of Regnase-1 expression in GFP$^+$ cells transduced with the indicated construct relative to cells transduced with GFP only calculated using gMFI (**d**). **e**, Structure of the Roquin-1 ROQ domain with a bound RNA stem loop marked in green, amino acid M199 marked in blue, amino acids essential for Roquin-1 and Regnase-1 functional interaction marked in orange and tested nonessential amino acids in yellow. **f**,**g**, WT (**f**) or iDKO (**g**) CD4$^+$ T cells were retrovirally transduced with GFP, GFP–roquin-1 or the indicated GFP–roquin-1 mutants. Histograms of ICOS, Regnase-1 and Ox40 expression in GFP$^+$ cells with indication of the

respective gMFI. Data are representative of $n = 3$ independent experiments (**a–c**,**f**,**g**) and are presented as mean ± s.e.m. of $n = 3$ independent experiments (**d**).

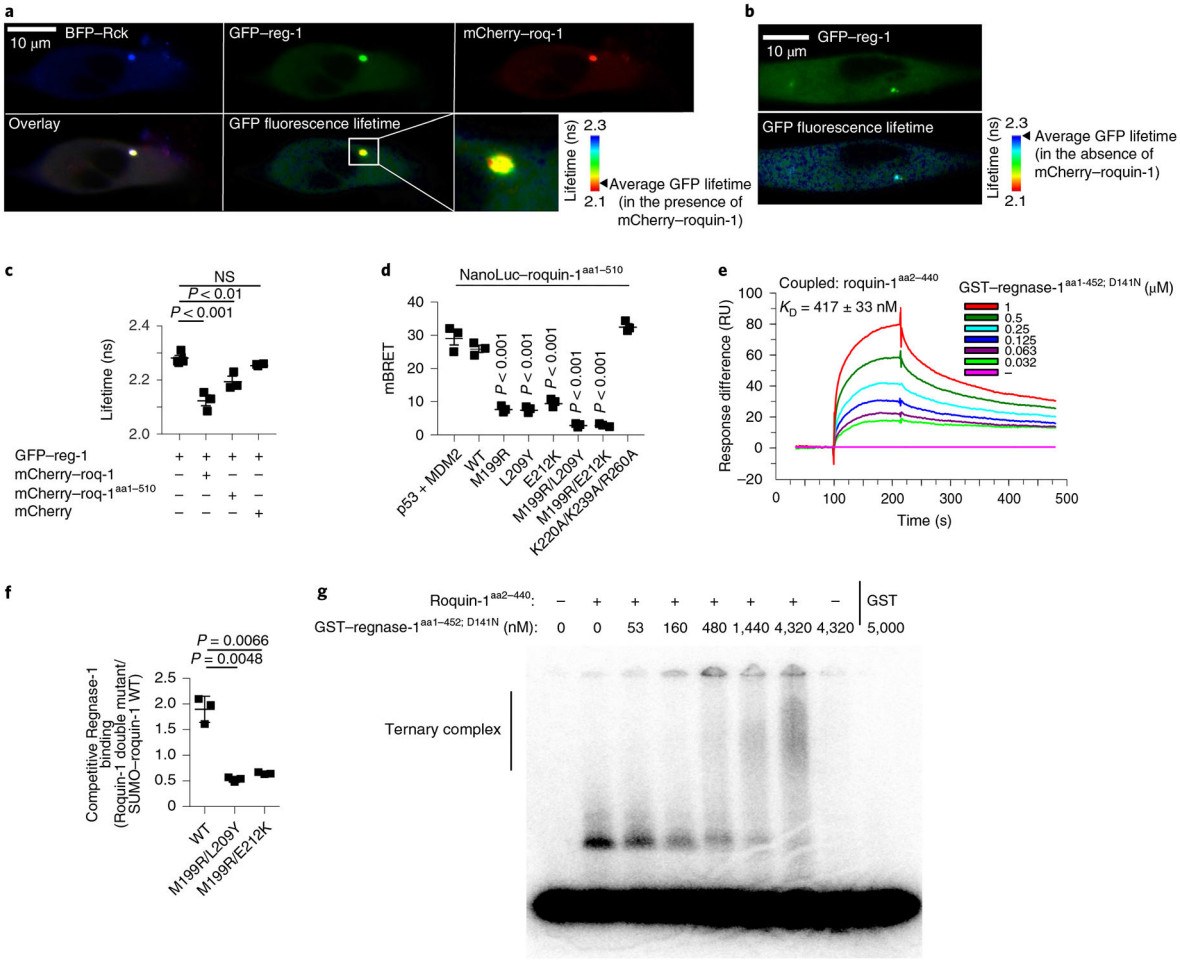

Fig. 5 | Molecular determinants of Roquin-1 interactions with Regnase-1.

a–c, HeLa cells were co-transfected with BFP–Rck, GFP–regnase-1 (GFP–reg-1) together with mCherry–roquin-1 (mCherry–roq-1), mCherry–roquin-1$^{aa1-510}$ or mCherry (**a**,**c**) or with GFP–regnase-1 alone (**b**). Protein localization (**a**,**b**), FRET efficiency (GFP–regnase-1 in combination with mCherry 0.67%, mCherry–roq-1 6.6% or mCherry–roq-1$^{aa1-510}$ 3.91%) and lifetime of GFP fluorescence (**c**) was analyzed via fluorescence lifetime microscopy. **d**, HEK293T cells were transfected with HaloTag–regnase-1 in combination with the indicated NanoLuc–roquin-1$^{aa1-510}$ expression plasmids and NanoBret ratio (mBRET) was calculated after measuring NanoLuc and HaloTag signals via NanoBret assay. **e**, SPR signals after addition of GST–regnase-1$^{aa1-452;D141N}$ to Biacore-chip-immobilized Roquin-1$^{aa2-440}$. RU, resonance units. **f**, Competitive in vitro GST-pulldown experiment using GST–regnase-1^{D141N} and wild-type SUMO–roquin-1$^{aa2-440}$ in combination with the indicated Roquin-1$^{aa2-440}$ double mutants (untagged). Quantification of eluted Roquin-1$^{aa2-440}$ mutant relative to SUMO–roquin-1$^{aa2-440}$ wild-type protein of SDS–PAGE depicted in Extended Data Fig. 7f. **g**, EMSA using a *Zc3h12a* 3′-UTR RNA fragment (nt194–212), Roquin-1$^{aa2-440}$ (320 nM) in combination with increasing levels of GST–regnase-1$^{aa1-452; D141N}$. Presumably due to inclusion of unlabeled competitor RNA, recognition of the *Zc3h12a* mRNA stem loop by Regnase-1 could not be detected.

Representative data of $n = 3$ independent experiments (**a**,**b**,**e**,**g**). Data are presented as mean ± s.e.m. of $n = 3$ independent experiments (**c**,**d**) or mean ± s.d. of $n = 3$ independent experiments (**f**). Statistical significance was calculated using one-way ANOVA with Bonferroni post hoc test (**c**,**d**) or Student's *t*-tests (**f**).

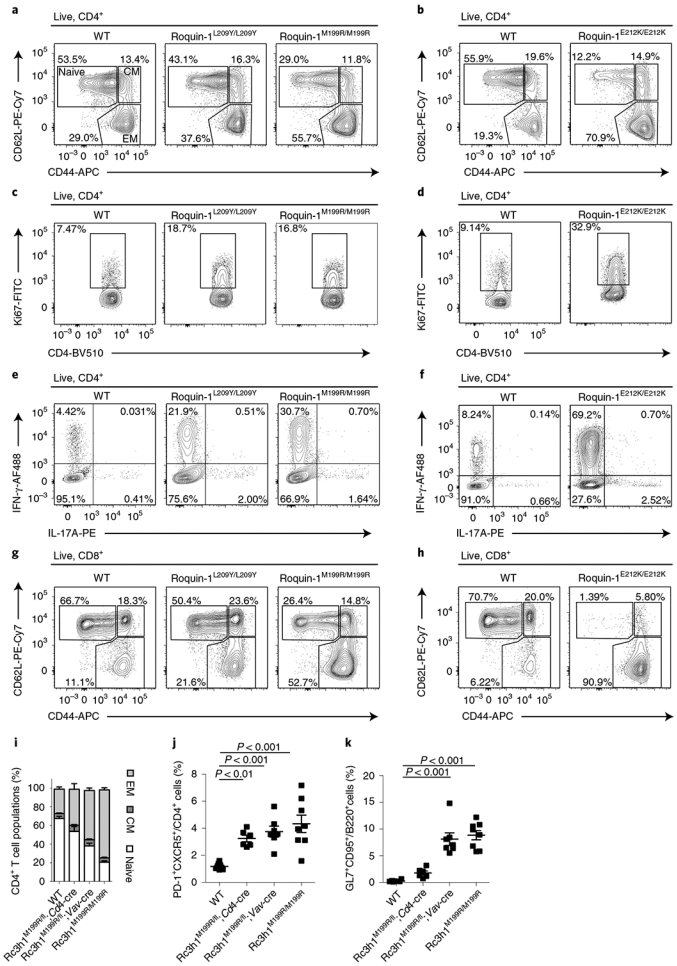

Fig. 6 | Inhibition of Roquin-1 interaction with Regnase-1 breaks T cell quiescence.

a–h, $CD4^+$ and $CD8^+$ T cells from mice with L209Y and M199R mutations (10–12 weeks old) or from mice with E212K mutations (8 weeks old) in Roquin-1 were characterized. $CD4^+$ effector/memory populations (**a**,**b**), $CD4^+$ T cell proliferation (**c**,**d**), ability of $CD4^+$ T cells to produce IFN-γ and IL-17 after PMA/ionomycin stimulation ex vivo (**e**,**f**) or $CD8^+$ effector/memory populations (**g**,**h**) were compared. **i–k**, Frequencies of $CD4^+$ effector/memory T cell populations (**i**), T_{FH} cells (**j**) and GC B cells (**k**) from spleens of 9–14-week-old WT, *Rc3h1*$^{M199R/fl}$;*Cd4*-Cre, *Rc3h1*$^{M199R/fl}$;*Vav*-Cre and *Rc3h1*$^{M199R/M199R}$ (*sanroque*) mice were determined by flow cytometry. Contour plots are representative of $n = 4$ biological replicates analyzed in at least two independent experiments (**a**,**c**,**e**,**g**) or $n = 2$ biological replicates in two independent experiments (**b**,**d**,**e**,**h**). Data are presented as mean ± s.e.m. of WT, *Rc3h1*$^{M199R/M199R}$, $n = 6$; *Rc3h1*$^{M199R/fl}$, *Cd4*-Cre, *Rc3h1*$^{M199R/fl}$, *Vav*-Cre, $n = 5$ (**i**) or WT, *Rc3h1*$^{M199R/M199R}$, $n = 8$; *Rc3h1*$^{M199R/fl}$, *Cd4*-Cre, $n = 6$; *Rc3h1*$^{M199R/fl}$, *Vav*-Cre, $n = 7$ (**j**,**k**) analyzed mice in at least three independent experiments. Statistical significance was calculated by one-way ANOVA with Bonferroni post hoc test (**j**,**k**).

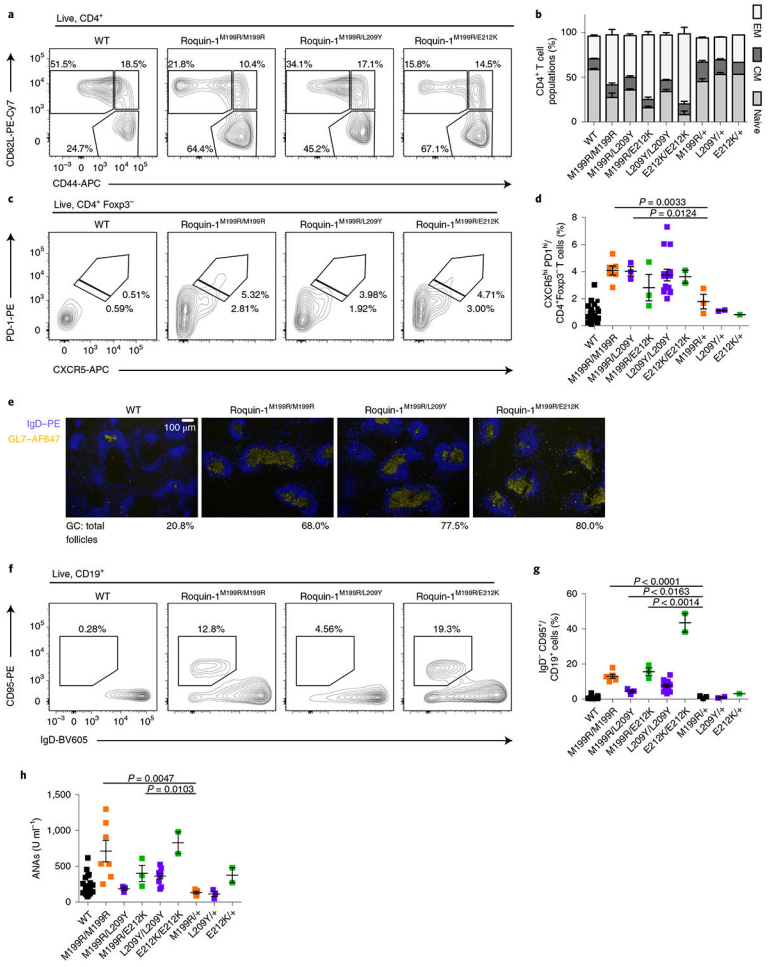

Fig. 7 | Combined heterozygosity of Roquin-1$^{E212K/M199R}$ shows a synthetic phenotype. **a–d,f–h**, T and B cells from 10–12-week-old mice with the M199R mutation in Roquin-1 on one allele and L209Y, E212K or M199R mutations on the other allele were characterized. Frequencies of CD4$^+$ T cell populations (**a**,**b**), T_{FH} cells (**c**,**d**), immunofluorescence of GL7 (blue) and IgD (yellow) in spleen sections (**e**), frequencies of GC B cells (**f**,**g**) and levels of ANAs in sera determined by ELISA (**h**). Contour plots or immunofluorescence microscopy images are representative of at least three individual mice analyzed in at least two independent experiments (**a**,**c**,**e**,**f**). WT, $n = 26$; M199R/M199R, $n = 6$; M199R/L209Y, $n = 3$; M199R/E212K, $n = 3$; L209Y/L209Y, $n = 14$; E212K/E212K, $n = 2$; M199R/+, $n = 3$; L209Y/+, $n = 2$; E212K/+, $n = 1$ (**b**,**d**,**g**,**h**). Data are shown as mean ± s.e.m. Statistical significance was determined using one-tailed Student's *t*-tests. Representative images of $n = 3$ analyzed mice per genotype (**e**).

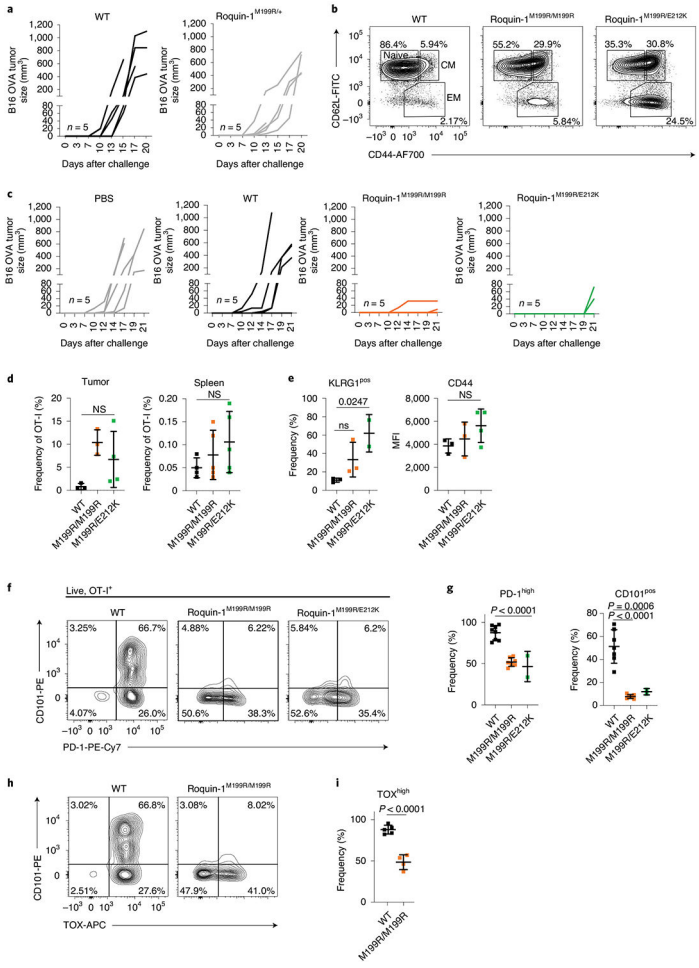

Fig. 8 |. Disrupting Roquin-1 interaction with Regnase-1 improves effector function of tumor-specific T cells.

a,c, Analysis of tumor growth of B16-OVA after transfer of OT-I T cells as described in Fig. 3i and with the indicated genotypes (n = 5 individual mice in one experiment, respectively). **b**, Flow cytometry analysis of activation markers CD44 and CD62L on OT-I T cells before transfer. **d**, Frequencies of OT-I T cells relative to all $^{+}$ cells are displayed for tumor and spleen at day 21 after tumor cell transfer. **e–i**, Flow cytometry analysis of KLRG-1, CD44, CD101, PD-1 and TOX on OT-I T cells in the tumor on day 21 after tumor cell transfer. Data are representative of WT, n = 4; M199R/M199R, n = 5; M199R/E212K, n = 5 individual mice analyzed in one experiment (**d**). Data are representative of WT, n = 3; M199R/M199R, n = 3; M199R/E212K, n = 2 or 4 each individual mice analyzed in one experiment (**e**). Data are representative of WT, n = 7; M199R/M199R, n = 7; M199R/E212K, n = 2 individual mice in three independent experiments (**g**). Data are representative of WT, n = 5 and M199R/M199R, n = 4 individual mice in two independent experiments (**h**). Data are presented as mean ± s.e.m. Statistical significance was calculated by one-way ANOVA with Bonferroni post hoc test (**d**,**e**,**g**) or unpaired one-tailed Student's t-test (**i**).